Title: Leveraging genetic diversity to identify small molecules that reverse mouse skeletal muscle insulin resistance

Authors: Stewart W.C. Masson, Søren Madsen, Kristen C. Cooke, Meg Potter, Alexis Diaz-Vegas, Luke Carroll, Senthil Thillainadesan, Ken Walder, Gregory J. Cooney, Grant Morahan, Jacqueline Stöckli and David E. James

Abstract

Systems genetics has begun to tackle the complexity of insulin resistance by capitalising on computational advances to study high-diversity populations. "Diversity Outbred in Australia (DOz)" is a population of genetically unique mice with profound metabolic heterogeneity. We leveraged this variance to explore skeletal muscle's contribution to whole-body insulin action through metabolic phenotyping and skeletal muscle proteomics of 215 DOz mice. Linear modelling identified 553 proteins that associated with whole-body insulin sensitivity (Matsuda Index) including regulators of endocytosis and muscle proteostasis. To enrich for causality, we refined this network by focussing on negatively associated, genetically regulated proteins, resulting in a 76-protein fingerprint of insulin resistance. We sought to perturb this network and restore insulin action with small molecules by integrating the Broad Institute Connectivity Map platform and *in vitro* assays of insulin action using the Prestwick chemical library. These complimentary approaches identified the antibiotic thiostrepton as an insulin resistance reversal agent. Subsequent validation in *ex vivo* insulin resistant mouse muscle, and palmitate induced insulin resistant myotubes demonstrated potent insulin action restoration, potentially via up-regulation of glycolysis. This work demonstrates the value of a drug-centric framework to validate systems level analysis by identifying potential therapeutics for insulin resistance.

23 **Introduction**

24 Skeletal muscle is a key determinant of whole-body glycaemic control. Under optimal conditions,
25 insulin secreted from the pancreas initiates a signalling program in muscle, and other tissues,
26 culminating in translocation of the insulin-responsive glucose transporter (GLUT4) to the plasma
27 membrane (1). Increased plasma membrane GLUT4 lowers circulating glucose by increasing cellular
28 influx for either storage as glycogen, or subsequent metabolism via the glycolytic pathway. Insulin
29 resistance is the progressive failure of these processes, and often precedes a number of metabolic
30 disorders including type 2 diabetes (2). Advances in genomics and computational biology have begun
31 to shed new light on molecular drivers of insulin resistance. A recent study in humans undertook a
32 GWAS of 188,577 individuals unveiling 53 genetic loci associated with a surrogate insulin resistance
33 signature (3). Such studies are important as they point toward genetic lesions in metabolic tissues like
34 skeletal muscle and adipose tissue as playing a key causal role in the development of insulin resistance.
35 This emphasises the importance of focusing on genetics and peripheral tissues for new therapeutic
36 targets and strategies to overcome insulin resistance. Recent developments in systems biology
37 provides unique opportunities for discovering ways of reversing and or preventing insulin resistance.
38 This will have enormous clinical benefit since insulin resistance is a gateway to an expanding family of
39 diseases.

40

41 Over the past decade, genetically diverse mouse panels have been used to study metabolic disease
42 (4-7). This is a major step forward because these panels combine control of the environment and
43 access to any biological tissue, with a vast phenotypic and range which can be leveraged towards
44 understanding complex diseases. Three specific resources are the hybrid mouse diversity panel
45 (HMDP), and the BXD (C57BL/6J x DBA) and Collaborative Cross (CC) mouse strains (7-11). These
46 panels comprise large selections of inbred mice spanning vast phenotypic and genetic landscapes.
47 Collaborative Cross mice were first generated by interbreeding five commonly used laboratory mouse

48 strains (C57BL/6J, A/J, 129S1/SvlmJ, NZO/HILtJ, NOD/ShiLtJ) and three wild-derived strains (WSB/EiJ,
49 CAST/EiJ, PWK/PhJ) in a 'funnel' design. The resulting CC strains were then outbred to generate
50 Diversity Outbred mice at Jackson Laboratories (12) which have increased phenotypic diversity and
51 resolution for genetic mapping. An independent Diversity Outbred colony was established in Western
52 Australia using CC mice from Geniad (13). This colony has since relocated to our group at The
53 University of Sydney, termed Diversity Outbred mice from Australia (Oz) or DOz.

54

55 The use of such rodent models for studying complex traits has given rise to the field of Systems
56 Genetics. System genetics uses global quantification of 'intermediate phenotypes' i.e., gene
57 transcripts, proteins, metabolites to provide mechanistic links between genetic variation and complex
58 traits/disease (14, 15). Unlike traditional genetic studies that identify single or multiple loci of interest,
59 systems genetics often identifies entire biological pathways or networks that are inherently more
60 difficult to empirically test. In an attempt to streamline interrogation of molecular pathways, several
61 large-scale perturbation screens/projects have been undertaken. One such example is the Broad
62 Institute's Connectivity Map that integrated mRNA expression levels from 1.5 million combinations of
63 different cell lines and perturbations (small molecule inhibitors, receptor ligands, genetic
64 manipulations) into a searchable database (16-19). These kinds of tools provide invaluable resources
65 for testing hypotheses generated from systems genetics experiments, and for broadly linking
66 molecular networks to phenotypic outcomes.

67

68 Here we have utilised DOz mice to interrogate insulin resistance. By combining metabolic phenotyping
69 and skeletal muscle proteomics we have identified an insulin resistance fingerprint of 76 proteins. We
70 then used Connectivity Map to identify small molecules that give rise to an overlapping transcriptional
71 signature across a number of cell lines, and therefore have the potential to affect insulin action.
72 Strikingly, one of these compounds, the antibiotic thiostrepton, was also identified by us in an

73 independent small molecule screen for effectors of insulin action in myotubes. Subsequent validation
74 of thiostrepton uncovered profound beneficial effects on insulin resistance *in vitro* and *ex vivo,*
75 potentially via modulation of mitochondrial function and glycolysis.

76

77 **Results**

78 *DOz metabolic and proteomic variation*

79 Diversity Outbred from Oz (DOz) mice were metabolically phenotyped by oral glucose tolerance test
80 (GTT) and echoMRI to determine body composition (Fig 1A-C). We integrated glucose and insulin
81 levels during the GTT into a surrogate measure of whole-body insulin sensitivity referred to as the
82 Matsuda Index (20). Similar to HOMA-IR, the Matsuda Index uses blood glucose and insulin values to
83 predict whole-body insulin sensitivity. However, an advantage of the Matsuda Index over HOMA-IR is
84 that it includes values over a range of GTT time-points, this better incorporates the dynamics of
85 glycaemic control. Furthermore, the Matsuda Index is better correlated to the euglycemic-
86 hyperinsulinaemic clamp, the gold standard measurement for insulin sensitivity, in humans (20).
87 Consistent with studies in other DO mouse populations (12, 21), we observed profound phenotypic
88 diversity in DOz mice with 20-to-400-fold differences in insulin sensitivity, adiposity, and fasting insulin
89 levels across all DOz animals (Fig 1C). Notably, the metabolic variation we observed in DOz mice is
90 markedly greater than the variation typically observed in similar studies using inbred mouse strains
91 (Fig 1D). Since skeletal muscle, and mitochondrial function are major contributor to whole body insulin
92 sensitivity in mammals (4, 22, 23), we performed proteomic analysis on quadriceps muscles that were
93 fractionated into mitochondrial and post-mitochondrial fractions (PMF, Fig 1A). We identified 2073
94 total proteins (444 mitochondrial and 1629 PMF) present in at least 50% of mice. Mitochondrial
95 proteins were defined based on their presence in MitoCarta 3.0 (24) and were two-fold enriched in
96 the mitochondrial fraction relative to the PMF (Fig 1E).

97

98 As with glycaemic control, muscle proteomes exhibited profound variation, with approximately 200-
99 fold differences in coefficient of variation (CV) across both fractions (Fig 1F). Interestingly,
100 glyceraldehyde-3-phosphate dehydrogenase (GAPDH), the often-reported western blot loading
101 control was the 11th most variable protein in our dataset. Amongst the other highly variable proteins
102 were the histone subunit H4F16, the mitochondrial iron-sulfur cluster assembly regulator ISCU, and
103 the metalloendopeptidase OMA1. Among proteins with low variability between mice was the
104 mitochondrial respiratory complex II subunit SDHA, and the 14-3-3 zeta isoform, YWHAZ. To uncover
105 how variation differed across biological processes, gene ontology (GO) enrichment analysis was
106 performed on proteins ranked by CV. Among the low variance processes were the electron transport
107 chain (mitochondrial fraction) and regulation of chromosome organisation (PMF), while lipid
108 metabolic pathways were highly variable across both mitochondrial and post-mitochondrial fractions
109 (Fig 1G).

110

111 *Role of skeletal muscle in whole-body insulin sensitivity*

112 To leverage genetic and metabolic diversity toward uncovering new regulators of insulin action, we
113 constructed linear models comparing insulin sensitivity (Matsuda Index) against protein abundance.
114 Our initial analysis identified 37 mitochondrial and 40 PMF proteins that significantly associated with
115 the Matsuda Index. Many of these appeared to be involved with adiposity rather than insulin action
116 including adiponectin (ADIPOQ), adipsin (CFD), and the mitochondrial β-oxidation proteins ETFA and
117 ETFB (Supplementary Fig 1a, b). Because we were mainly interested in identifying muscle-specific
118 factors that regulate insulin sensitivity, we next constructed a model that included adiposity (the
119 percentage of body mass which is adipose tissue) as a covariate. Using this approach, we identified
120 120 mitochondrial (Fig. 2A-B) and 433 PMF proteins that significantly associated with whole-body
121 insulin sensitivity. Comparison of the results from each model (with and without adiposity as a

122 covariate), revealed consensus proteins that associated with insulin sensitivity independently of
123 model design (Supplementary Fig 1C). These included the glycolytic enzymes PFKFB1 and PKM, which
124 have previously been identified as regulating muscle insulin action (4). Using adiposity as a covariate
125 not only increased the number of proteins identified but also uncovered relationships between
126 Matsuda Index and the GLUT4 trafficking regulators RAB10 (25, 26), SNAP23 (27) and IQGAP1 (28)
127 which were not seen in the original model. Comparison of the mitochondrial and PMF proteomes
128 revealed a mitochondrial enrichment for proteins that positively associate with insulin sensitivity,
129 highlighting the broadly positive role mitochondria play in muscle's contribution to metabolic health
130 (Fig 2C).

131

132 To gain further insight into the biology of skeletal muscle glycaemic control, we annotated candidate
133 proteins with PhosphoSite Plus data to test whether any protein of interest had documented roles in
134 metabolic signalling (Fig 2D-F). We observed no relationship between insulin signalling substrates and
135 regulation of whole-body insulin sensitivity (Fig 2D). However, there was a trend ($p = 0.08$) for AMPK
136 substrates in the PMF to be positively associated with insulin sensitivity. Interestingly, the most
137 positively (Canopy2; CNYP2) and most negatively (Rho GDP dissociation inhibitor alpha; ARHGDIA)
138 associated proteins were both annotated as being insulin responsive (Fig. 2F). We also preformed GO
139 gene-set enrichment analysis (GSEA) on proteins ranked by Matsuda Index effect sizes (Fig 2G). In the
140 PMF, 'response to topologically incorrect protein: GO:0051788' was positively associated with insulin
141 sensitivity while the 'proteasome complex: GO:0005839' and 'clathrin-coated pit: GO:0005905' were
142 negatively associated. Together the unfolded protein response and proteasome are indicative of the
143 role of proteostasis in insulin sensitivity (29, 30). Conversely, clathrin-coated pits play an important
144 role in the internalisation of the insulin sensitive glucose transporter GLUT4 from the cell surface, a
145 process negatively regulated by insulin (31-33). Consistent with our observation that the majority of
146 the mitochondrial proteome is positively associated with insulin sensitivity, GSEA did not produce any

147 negative results but did uncover a positive relationship between the mitochondrial respiratory
148 complex I and Matsuda Index.

149

150 *Integration of genetic linkage analysis and linear modelling with Connectivity Map*

151 Changes in protein levels may be either cause or consequence of changes in insulin sensitivity. In an
152 attempt to select for proteins with a potentially causal relationship, we performed genetic mapping
153 analysis of both the mitochondrial and PMF proteomes (Fig 3A). Across both proteomes we identified
154 624 protein quantitative trait loci (pQTL). Of these, 400 were cis acting indicating that a significant
155 proportion of variation in these proteins can be explained by their local genetic architecture. Next, we
156 filtered proteins that were negatively associated with Matsuda Index by cis-pQTL presence to generate
157 a molecular fingerprint of insulin resistance (Fig 3B). We focussed on negatively associated proteins
158 based on the assumption that inhibiting deleterious proteins is easier than promoting the activity of
159 beneficial ones. Our analysis yielded a list of 76 (69 PMF and 7 mitochondrial) proteins that
160 encompassed a wide range of biological processes (Supplementary Table 1). Similar approaches to
161 identify molecular phenotypes of insulin resistance have previously been conducted using collated
162 human transcriptomic datasets (34-44). Using a compiled list from Timmons et al (45), we searched
163 for orthologues of proteins from our fingerprint that associate with human insulin resistance. We
164 identified four such genes (Fig. 3B): MTPN (myotrophin), LGALS1 (galectin 1), PHKB (phosphorylase b
165 kinase), and ADPRHL1 (ADP-ribosylhydrolase Like 1), which may warrant further investigation. We also
166 queried our fingerprint for any biological pathways that could represent novel drivers of insulin
167 resistance by performing KEGG pathway enrichment (Fig 3C). Both 'endocytosis: mmu04144' (clathrin
168 light chain A, clathrin light chain C, epidermal growth factor receptor pathway substrate 15) and
169 'insulin signalling pathway; mmu04910' (phosphorylase kinase regulatory subunit beta) featured in
170 the top 10 providing further supportive evidence for the biological relevance of our fingerprint in the
171 context of insulin sensitivity.

172

173 Next, we utilized Connectivity Map (CMAP) to convert our fingerprint into a list of small molecules and
174 ligands that promote or oppose our muscle insulin resistance fingerprint. To test our assumption that
175 pQTL filtering would improve our fingerprint we also queried CMAP with a list of the top 150 most
176 strongly negatively associated proteins independent of pQTL presence. Intriguingly, on average CMAP
177 scores for compounds and ligands were significantly higher when captured using a pQTL-filtered
178 fingerprint compared to the non-pQTL filtered group, supporting the utility of this method
179 (Supplementary Figure 2A). Encouragingly, the two highest scoring compounds identified using our
180 fingerprint were Broad Institute glycogen synthase kinase (GSK3) and epidermal growth factor
181 receptor (EGFR) inhibitors. Both of these kinases have been independently identified as drug targets
182 that reverse insulin resistance (36, 46, 47). Many compounds listed in the Connectivity Map database
183 are proprietary Broad Institute inhibitors which are only identified by their Broad ID and cannot be
184 easily procured for follow-up experiments. Therefore, we excluded all Broad Institute compounds
185 from further analysis. After this filtering, 856 small molecules and 91 ligands generated gene
186 expression signatures matching our query. As whole-body insulin sensitivity decreased with increased
187 fingerprint protein abundance, we focussed on molecules whose CMAP score suggested a reversal of
188 our insulin resistance fingerprint (Fig 3D). Ranking these candidates based on CMAP score revealed a
189 number of well-known potentiators of insulin sensitivity including the antioxidant resveratrol (48), the
190 diabetes medication metformin (49) and the growth factor FGF21 (50). We also identified the
191 antibiotic thiostrepton (51), a documented proteasome inhibitor, consistent with our enrichment
192 analysis which identified the proteasome as negatively contributing to insulin sensitivity.

193

194 *Cross-validation of thiostrepton by Prestwick library screen of GLUT4 translocation*

195 To obtain independent validation of some of the candidates revealed from Connectivity Map we
196 performed a screen for compounds that affect GLUT4 translocation to the cell surface in L6 myotubes

197 expressing HA-tagged GLUT4 (GLUT4-HA-L6), a readout of insulin action that is defective in insulin
198 resistance. For this we used our established high sensitivity, high-throughput 96-well plate format
199 screen that is amenable to physiological models of insulin resistance (52, 53), combined with the
200 Prestwick library of FDA-approved drugs since this library was also part of the CMAP analysis pipeline.
201 We performed 3 separate screens (Fig 4A) to capture the different mechanisms by which compounds
202 modulate glucose uptake: 1) insulin-independent activation of GLUT4 translocation to the plasma
203 membrane (basal activators), 2) potentiation of submaximal insulin action (insulin sensitisers), and 3)
204 rescue of palmitate-induced insulin resistance (insulin resistance reversers). We identified 22 basal
205 agonists (Fig 4B), 7 insulin sensitisers (Fig 4C) and 16 insulin resistance reversers (Fig 4D). Five
206 compounds both stimulated GLUT4 translocation and reversed insulin resistance, 4 were both basal
207 agonists and insulin sensitisers while none met all three criteria (Fig 4E). Overall, we found that
208 compounds that were identified by CMAP score (Fig 3D) performed better as both basal activators
209 and as insulin resistance reversers than those that did not (Supplementary Fig 2B).

210

211 To cross-reference our CMAP data with the Prestwick screen in an unbiased way, we constructed a
212 scoring matrix to rank compounds found by both our CMAP query and in the Prestwick library. First,
213 we z-scored the values for each category (basal agonists, insulin sensitisers, insulin resistance reversal,
214 CMAP score). Next, we averaged the three *in vitro* assays z-scores and added it to the CMAP score.
215 This overall score represents how each compound modulates GLUT4 translocation, and potentially
216 reverses our insulin resistance fingerprint, relative to the rest of the compound library. Using this final
217 value, we ranked each compound and displayed the top 20 in a heat map (Fig 5A). Based on this
218 metric, thiostrepton was identified as the highest-ranking compound and was selected for subsequent
219 validation by further GLUT4 translocation (Fig. 5B) and 2-deoxyglucose uptake (Fig. 5C) experiments
220 in GLUT4-HA-L6 myotubes. We observed a consistent reversal of insulin resistance across both assays.

221

222 Next, we assessed the efficacy of thiostrepton to reverse insulin resistance in diet-induced obese mice.
223 We decided to study it in isolated muscles as this circumvents potentially confounding microbiome
224 effects due to thiostrepton's antibiotic activity and allows direct interrogation of muscle insulin action.
225 We selected two strains of inbred mice, C57BL/6J and BXH9/TyJ, based on our previous observations
226 that these strains are particularly amenable to developing muscle insulin resistance following high-fat,
227 high-sugar (western diet; WD) diet feeding (4). Consistent with diet-induced perturbations in
228 metabolic health, both C57BL/6J and BXH9 BXH9/TyJ mice fed a WD had increased body weight and
229 adiposity, fasting hyperglycemia, fasting hyperinsulinemia, glucose intolerance and lower systemic
230 insulin sensitivity (Matsuda Index) relative to chow-fed controls (Supplementary Fig. 3A-E). WD
231 feeding also resulted in ~40% reduction in C57BL/6J soleus insulin stimulated 2-deoxyglucose uptake,
232 a 75% reduction in BXH9 extensor digitorum longus insulin-stimulated 2-deoxyglucose uptake and
233 65% reduction in BXH9 soleus insulin stimulated 2-deoxyglucose uptake. Strikingly, 1 h of thiostrepton
234 treatment prior to insulin addition was sufficient to reverse 80% of WD-induced insulin resistance in
235 C57Bl/6J EDL muscle and 50% in BXH9 EDL muscle but did not restore BXH9 soleus 2-deoxyglucose
236 uptake (Figure 5D).

237

238 *Thiostrepton does not affect insulin signalling*

239 Next, we attempted to identify the potential mechanisms by which thiostrepton relieved insulin
240 resistance. Canonically, insulin stimulated GLUT4 translocation is facilitated by a signalling cascade
241 comprising PI3K/Akt and dysfunction in this pathway has been implicated in insulin resistance (54),
242 although this is controversial (2). To assess insulin signalling we treated control and palmitate-treated
243 GLUT4-HA-L6 myotubes with either thiostrepton or vehicle for 1 h prior to insulin stimulation. Unlike
244 GLUT4 translocation or 2-deoxyglucose uptake, palmitate did not perturb proximal insulin signalling.
245 We detected no effect of palmitate treatment or thiostrepton on the phosphorylation of Akt-T308,
246 Akt-S473, or the Akt-substrates GSK3-S21/9 and PRAS40-T246 (Fig. 6A-E). These findings are

247 consistent with the view that insulin resistance occurs independently of canonical insulin signalling
248 (55, 56) and suggests that thiostrepton is acting independently of signalling to reverse insulin
249 resistance.

250

251 *Thiostrepton partially inhibits mitochondria and restores palmitate induced glycolysis suppression*

252 Many insulin sensitising agents act via mitochondrial inhibition or uncoupling (57-59) and thiostrepton
253 has been reported to inhibit mitochondrial translation (60) and respiration (61, 62). To test whether
254 thiostrepton's ability to restore optimal insulin action occurs via mitochondria, palmitate-treated and
255 control GLUT4-HA-L6 myotubes were incubated with thiostrepton as above. Consistent with the
256 mitochondrial dysfunction that has been reported during insulin resistance (23, 63), we observed
257 substantial suppression of maximal mitochondrial respiration and mitochondrial reserve capacity
258 following palmitate treatment (Fig. 7A). Furthermore, thiostrepton alone appeared to blunt maximal
259 respiration, albeit to a lesser extent than palmitate. When combined, thiostrepton and palmitate did
260 not produce an additive suppression, nor did thiostrepton reverse any of the palmitate-induced
261 defects. This suggests that this suppression of maximal respiration does not contribute to insulin
262 resistance in this model.

263

264 We also assessed glycolysis by way of extra-cellular acidification rate (ECAR). Like mitochondrial
265 respiration, palmitate suppressed maximal glycolytic capacity, however unlike respiration this was
266 potently reversed by co-treatment with thiostrepton (Fig. 7B). To test whether this increase in
267 glycolytic flux could be explained by changes in cellular energy status due to mitochondrial inhibition,
268 we investigated the energy sensor AMP-dependent kinase (AMPK). AMPK can promote glycolysis (64),
269 GLUT4 translocation (65, 66), and glucose uptake in skeletal muscle independently of insulin.
270 However, unlike the AMPK activator A-769662, we observed no effect of thiostrepton on the

271 phosphorylation of AMPK or its substrate acetyl-CoA carboxylase in either control cells or cells treated
272 overnight with palmitate (Fig. 7C-E). Although A-769662 potently increases AMPK substrate
273 phosphorylation in muscle cells, AMPK phosphorylation itself is not observed, consistent with a
274 previous study (67). These data suggest that if thiostrepton activates glycolysis via mitochondrial
275 inhibition, it occurs independently of AMPK.

276

277 **Discussion**

278 By leveraging genetic and phenotypic diversity of DOz mice we have explored skeletal muscle's
279 contribution to whole-body insulin action at the molecular level. Our approach was validated by the
280 identification of various 'positive controls' at each level of analysis. Firstly, utilising adiposity as a
281 covariate during linear modelling uncovered relationships between whole-body insulin sensitivity and
282 muscle GLUT4 trafficking proteins; secondly, pathway enrichment revealed proteostasis (29, 68) and
283 endocytosis (31, 69) as key contributors to whole-body insulin sensitivity; and thirdly, querying
284 Connectivity Map with our fingerprint of insulin resistance returned metformin, GSK3 (36, 70) and
285 EGFR (46) inhibitors as potential insulin resistance therapeutics (49). The identification of these
286 proteins, pathways and drugs by our strategy gives us confidence in our approach and the novel
287 players identified.

288

289 Systems-based approaches often identify networks as being drivers of disease. Empirical validation of
290 these is difficult due to the complex interactions in biological systems. Here we took a drug-centric
291 approach to validate our findings; this allowed targeting of entire pathways rather than singular
292 nodes. We identified several compounds across both *in silico* and *in vitro* analyses which may restore
293 muscle insulin action, indeed several of these have previously been investigated. Disulfiram, sold
294 under the brand name Antabuse, is used as an alcohol-dependency medication. Two studies have

295 described disulfiram's ability to reverse diet-induced hepatic insulin resistance and reduce adiposity
296 (71, 72). Resveratrol, a component found in red wine, is a popular antioxidant and has been
297 demonstrated to reverse insulin resistance via reduction of reactive oxygen species (48, 73, 74).
298 Fibroblast growth factor 21 (FGF21) was also identified amongst the ligand dataset as reversing our
299 insulin resistance fingerprint. FGF21 has previously been reported to promote insulin-stimulated
300 glucose uptake in muscle fibres (75) and can modulate mitophagy and proteostasis in muscle (76).
301 Antivirals, several classes of antibiotics, antipsychotics and cancer drugs were all identified by our
302 analyses. Perhaps this diversity reflects the divergent and pleiotropic biology of insulin resistance.

303

304 Key to our approach is the insulin resistance muscle proteomic fingerprint. This was generated by
305 filtering proteins that associated with whole-body insulin sensitivity and that possessed significant cis-
306 pQTLs. The latter was particularly important as we postulated that this would select for proteins that
307 were likely to be causal drivers of insulin resistance. We hypothesed that a protein whose expression
308 is post-translationally regulated in response to insulin resistance would not show a genetic signal and
309 therefore be excluded from our fingerprint. Filtering on this basis improved the overall Connectivity
310 Map score, and ultimately identified thiostrepton. One reason for this could be the discordance
311 between mRNA and protein (77, 78). Connectivity Map uses mRNA expression data whereas our
312 fingerprint uses protein. By restricting our fingerprint to proteins with significant pQTLs we may have
313 inadvertently selected for genes whose mRNA expression closely matches their protein thereby
314 increasing the overlap between fingerprint and perturbagen signatures. While this approach is less
315 powerful than QTL co-localisation for identifying causal drivers, it has the major advantage that it
316 requires a much reduced sample size (222 mice in this study) compared to the 400-600 mice which
317 would be required for complex trait genetic mapping (79).

318

319 A major question is what biological functions are represented by our fingerprint? One of the top
320 pathways identified was endocytosis. This pathway featured two components of the clathrin coat and
321 the adaptor protein EPS15. This is very exciting as endocytosis has been suggested to play a major role
322 in stress signalling (80), and in the context of insulin sensitivity this may involve internalisation of key
323 proteins including the insulin receptor and glucose or amino acid transporters (31, 69). The concept
324 that variation in this process is genetically determined, and this plays a major role in governing
325 essential processes like insulin action, adds a new dimension to the role of this pathway. A second
326 intriguing member of the fingerprint is phosphorylase kinase which, along with glycogen synthase
327 kinase, regulates the key glycogen storage enzymes glycogen phosphorylase and glycogen synthase
328 (81-84). High levels of glycogen phosphorylase kinase may promote glycogen breakdown through
329 activation of glycogen phosphorylase thereby altering GSK3 signalling, a process implicated in insulin
330 resistance.

331

332 Neither AMPK nor Akt signalling account for the profound effect of thiostrepton on insulin action. This
333 is exciting as it suggests both a novel mechanism of action and a novel insulin resistance defect. So
334 far, the most enticing potential mechanism is restoration of glycolysis. Thiostrepton restores normal
335 glycolytic function in palmitate treated cells and we have previously reported links between glycolysis
336 and insulin action in skeletal muscle across a diverse panel of mouse strains (4). Furthermore,
337 potentiation of glycolysis has been linked to increases in insulin signalling via Akt (85). Mechanistically,
338 thiostrepton could promote glycolysis via attenuation of mitochondrial oxidative phosphorylation,
339 and this has previously been demonstrated in acute myeloid leukemia and malignant mesothelioma
340 cell lines (61, 86). Our data supports this work and identifies a similar, albeit mild, effect on myotube
341 respiration. Thiostrepton can also increase cellular exposure to mitochondrial reactive oxygen species
342 (ROS) as it inhibits peroxiredoxin-3 (62, 86), a key antioxidant enzyme. Perhaps, as seen during the

343 Warburg effect (87-89), increased mitochondrial ROS can act as a signal to promote glycolysis and
344 relieve mitochondrial energetic demands.

345

346 Integration of physiological, proteomic, genomic, and pharmaceutical data has uncovered a potent
347 reverser of insulin resistance. By integrating proteomic diversity with the underlying genetic
348 architecture, we believe we were able to focus on potentially causal proteins, and the use of
349 Connectivity Map allowed us to combine these proteins into a single fingerprint to find potential
350 modulators of insulin resistance. Our findings also build on recent reports linking glycolysis to insulin
351 action and uncover a number of potential contributors to insulin action worthy of future study.

352

353 **Methods**

354 Mouse breeding and phenotyping

355 Male Diversity Outbred from Oz (DOz) mice were bred and housed at the Charles Perkins Centre,
356 University of Sydney, NSW, Australia. They were originally established at Geniad, Western Australia,
357 Australia and then relocated to The University of Sydney. The DOz population comprises 46 breeding
358 pairs and the breeding strategy avoids mating's between siblings or first cousins. Breeders are selected
359 based on the genotype of the *R2d2* locus to limit the meiotic drive favouring the WSB allele on
360 chromosome 2 (90). The DOz mice used in the current study were outbred for 27 to 33 generations
361 and comprised a total of 250 male DOz mice that were studied as 5 separate cohorts. Genomic DNA
362 was isolated from each mouse and subjected to SNP genotyping (91), followed by genotyping
363 diagnostics and cleaning as described (92). Experiments were performed in accordance with NHMRC
364 guidelines and under approval of The University of Sydney Animal Ethics Committee. To delineate
365 genetic from cage-effects, mice were randomised into cages of 3-5 at weaning. All mice were
366 maintained at 23°C on a 12-hour light/dark cycle (0600-1800) and given *ad libitum* access to a standard
367 laboratory chow diet containing 16% calories from fat, 61% calories from carbohydrates, and 23 %
368 calories from protein or a high-fat high-sugar diet (western diet; WD) containing 45% calories from
369 fat, 36% calories from carbohydrate and 19% calories from protein (3.5%g cellulose, 4.5%g bran, 13%g
370 cornstarch, 21%g sucrose, 16.5%g casein, 3.4%g gelatine, 2.6%g safflower oil, 18.6%g lard, 1.2%g AIN-
371 93 vitamin mix (MP Biomedicals), 4.95%g AIN-93 mineral mix (MP Biomedicals), 0.36%g choline and
372 0.3%g L-cysteine). Fat and lean mass measures were acquired via EchoMRI-900 (EchoMRI Corporation
373 Pte Ltd, Singapore) at 14 weeks of age. Glucose tolerance was determined by oral glucose tolerance
374 test (GTT) at 14-weeks of age by fasting mice for 6-hours (0700-1300 hrs) before oral gavage of 20%
375 glucose solution in water at 2 mg/kg lean mass. Blood glucose concentrations was measured directly
376 by handheld glucometer (Accu-Chek, Roche Diabetes Care, NSW, Australia) from tail blood 0, 15, 30,
377 45, 60, 90 minutes after oral gavage of glucose. Blood insulin levels at the 0- and 15-minute time points
378 were measured by mouse insulin ELISA Crystal Chem USA (Elk Grove Village, IL, USA) according to

379 manufacturer instructions. Blood glucose and insulin levels were integrated into a surrogate measure
380 of whole-body insulin sensitivity using the Matsuda Index:

381

382 $$Matsuda\ Index = \frac{10{,}000}{\sqrt{(Glucose_0 \times\ Insulin_0) \times (Glucose_{\mathrm{GTT}\ mean} \times\ Insulin_{GTT\ mean})}}$$

383

384 Muscle proteomic sample prep

385 Whole quadriceps muscle was snap frozen with liquid nitrogen and pulverized before resuspension in
386 100 µL of trypsin buffer (phosphate buffered saline; PBS containing 10 mM EDTA and 0.01 ug/uL mass-
387 spectrometry grade trypsin). Samples were incubated for 30 minutes at 37 °C before being pelleted
388 by centrifugation (10,000 g, 5 minutes at 4 °C). Samples were then resuspended in 1.4 mL
389 mitochondrial isolation buffer (70 mM sucrose, 220 mM Mannitol, 1 mM EGTA, 2 mM HEPES. pH at
390 7.4) and homogenised on ice in a glass Dounce homogeniser. Samples were then twice pelleted by
391 centrifugation, first at 1000 g x 10 min to remove insoluble debris and second at 10,000 g x 10 min to
392 extract the crude mitochondrial fraction, both centrifugation steps were performed at 4 °C and the
393 supernatant of the second step was collected as the post-mitochondrial fraction (PMF). The
394 mitochondrial pellet was re-solubilised in 1 mL of isolation buffer by repeated pipetting on ice prior to
395 centrifugation (10.000 g x 10 min at 4*C) and resuspension in 50 µL of isolation buffer. Protein
396 concentration of both mitochondrial and PMF was determined by BCA assay, 10 µg of protein was
397 then prepared as previously described (4). Reduction/alkylation (10mM TCEP, 40mM CAA) buffer was
398 added to each sample before incubation for 20 minutes at 60 °C. Once cooled to room temperature,
399 0.4 mg trypsin and 0.4 mg LysC was added to each sample and incubated overnight (18h) at 37C with
400 gentle agitation. 30µL water and 50 µL 1% TFA in ethyl acetate was added to stop digestion and
401 dissolve any precipitated SDC. Samples were prepared for mass spectrometry analysis by StageTip
402 clean up using SDB-RPS solid phase extraction material (93). Briefly, 2 layers of SDB-RPS material was

403 packed into 200 µL tips and washed by centrifugation at 1,000 x g for 2 minutes with 50 µL acetonitrile
404 followed by 0.2% TFA in 30% methanol and then 0.2% TFA in water. 50 µL of samples were loaded to
405 StageTips by centrifugation at 1,000 g for 3 minutes. Stage tips were washed with subsequent spins at
406 1,000 g for 3 minutes with 50 µL 1% TFA in ethyl acetate, then 1% TFA in isopropanol, and 0.2% TFA
407 in 5% ACN. Samples were eluted by addition of 60µL 60% ACN with 5% NH_4OH_4. Samples were dried
408 by vacuum centrifugation and reconstituted in 30 µL 0.1% TFA in 2% ACN.

409

410 Mass spectrometry analysis

411 Proteomic sample analysis was conducted using a Dionex UltiMate 3000 RSLCnano LC coupled to a
412 Exploris Orbitrap mass spectrometer. 2 µL of sample was injected on to an in-house packed 150 µm x
413 15 cm column (1.9 mm particle size, ReproSilPurC18-AQ) and separated using a gradient elution and
414 with column temperature of 60 °C, with Buffer A consisting of 0.1% formic acid in water and Buffer B
415 consisting of 0.1% formic acid in 80% ACN. Samples were loaded to the column at a flow rate 3 µL min^{-}
416 ^{1} at 3% B for 3 minutes, before dropping to 1.2 µL min^{-1} over 1 minute for the gradient elution. The
417 gradient was increased to 32% B over 50 min, then to 60% B over 0.5 min and 98% B over 0.5 min and
418 held for 1.5 min, before returning to a flow rate of 3 µL min^{-1} at 3% B. Eluting peptides were ionized
419 by electrospray with a spray voltage of 2.3kV and a transfer capillary temperature of 300 °C. Mass
420 spectra were collected using a DIA method with varying isolation width windows (widths of *m/z* 22-
421 589) between 350 - 1650 according to Table S1. MS1 spectra were collected between *m/z* 350-1650
422 at a resolution of 60,000 and an AGC target of 4e5 with a 50 ms maximum injection time. Ions were
423 fragmented with stepped HCD collision energy at 27.5% and MS2 spectra collected between m/z 300-
424 2000 at resolution of 30,000, with an AGC target of 3e5 and the maximum injection time of 54 ms.

425

426 Proteomics raw data files were searched using DIA-NN using a library free FASTA search against the
427 reviewed UniProt mouse proteome (downloaded May 2020) with deep learning enabled (93, 94). The
428 protease was set to Trypsin/P with 1 missed cleavage, N-term M excision, carbamidomethylation and
429 M oxidation options on. Peptide length was set to 7-30, precursor range 350-1650, and fragment range
430 300-2000, and FDR set to 1%. Both the PMF and mitochondrial fractions were filtered for
431 mitochondrial proteins using based on MitoCarta 3.0 and presence in 50% in mice. Across both
432 fractions we quantified 2073 proteins (1629 proteins in the PMF and 444 in the mitochondrial
433 fraction). Proteomic intensities were log2 transformed and median normalised prior to analysis.

434

435 Data analysis

436 All data analysis and visualisation was performed in either the R programming environment (95) or
437 GraphPad Prism (GraphPad Software, San Diego, California USA). For protein-trait analysis the
438 Matsuda Index was calculated using glucose tolerance data before being log2 transformed. Linear
439 models were generated using the *lm()* function in R where Matsuda Index = α + proteinX + covariate
440 + ε (α = intercept and ε = error) using a gaussian distribution. To correct for multiple testing, p-values
441 were adjusted using the q-value method in the R package *qvalue* (96). Chi-square tests for distribution
442 differences within the data and two/one-way ANOVA tests for group differences were performed in
443 GraphPad Prism.

444

445 Gene-set enrichment

446 Gene-set enrichment analysis for each mitochondrial and post-mitochondrial fraction was conducted
447 using Matsuda Index effect sizes for each protein and performed in R using the *gseGO()* function within
448 the clusterprofiler package (97). Over-representation analysis of protein-protein interaction clusters
449 and KEGG pathway analysis of insulin resistance fingerprint proteins were performed in WebGestalt

450 (98). All enrichment tests were performed using all quantified proteins within a given fraction as a
451 background gene-set. P-value correction was performed using false-discovery rate correction.

452

453 Genetic mapping analysis

454 Genetic mapping analysis was performed in R using the QTL2 package (99). The GIGA-MUGA single
455 nucleotide polymorphism array was used as genomic inputs for mapping (91). pQTL analysis was
456 performed by linear mixed modelling on z-scored protein abundance data with probabilistic
457 estimation of expression residuals (PEER) factor adjustment, a covariate, and a kinship matrix to
458 account for genetic relatedness amongst the DOz animals. PEER factor adjustment was performed
459 using the top 10 calculated PEER factors, as described (100). Significance thresholds were established
460 by performing 1000 permutations and set at $P < 0.1$ for cis-acting pQTL and $P < 0.05$ for trans acting
461 pQTL. The cis-pQTL window was set as ± 2 Mbp.

462

463 Connectivity Map and scoring matrix

464 Insulin resistance 'fingerprint' proteins were queried in Connectivity Map using the CLUE software
465 platform (16, 19). The list of 76 'fingerprint proteins' were queried against the L1000 gene expression
466 dataset in the "Query" function of CLUE and results for small molecules (trt_cp) and ligands (trt_lig)
467 were extracted using the CLUE "Morpheus" platform. Raw connectivity score values were used to rank
468 perturbagens. Connectivity scores were averaged across all cell lines in the L1000 dataset. The Broad
469 Institute small molecule inhibitors denoted by the prefix were removed from our resulting dataset as
470 they are not commercially available. Connectivity Map scores were combined with the results from
471 our GLUT4 translocation screen to rank consensus compounds. This was done by first z-scoring each
472 value (% GLUT4 at the plasma membrane for each assay and raw connectivity score). This produced a
473 value which indicates how well each compound performs in a given test relative to the rest of the

474 dataset. Then the average of all three GLUT4 assays (basal agonism, insulin sensitisation, and insulin
475 resistance reversal) was added to the z-scored Connectivity Score to produce an overall score for each
476 compound. Z-score adjustment for each assay and CMAP score was performed as follows:

477 $$Zscore = \frac{x - mean}{SD}$$

478 Where:

479 - Zscore = adjusted value for a given compound
480 - x = observed score for given compound
481 - mean = average score across all compounds
482 - SD = standard deviation of all compounds

483 Overall score for each compound was calculated as follows:

484 $$\frac{\text{z-scored }(bas) + \text{ z-scored }(ins.sens) + \text{z-scored }(ins.res.rev)}{3} + \text{ z-scored }(CMAP)$$

485 $$= Overall\ score$$

486 Cell culture

487 GLUT4-HA-L6 myoblasts (101) were grown in α-MEM supplemented with 10% fetal bovine serum.
488 Differentiation was induced by changing media to α-MEM supplemented with 2% horse serum for 5
489 days.

490

491 GLUT4 translocation assays

492 GLUT4 exocytosis was determined as previously reported (52). Briefly, GLUT4-HA-L6 myotubes were
493 serum starved overnight in α-MEM containing 0.2% BSA before being washed 3x with Krebs Ringer
494 phosphate buffer supplemented with 0.2% BSA. Cells were stimulated with either 1 nM or 100 nM
495 insulin for 20 minutes before being washed with ice-cold PBS and placed on ice. Cells were then fixed

496 for 30 minutes in 3% paraformaldehyde, washed with phosphate buffered saline. Remaining
497 paraformaldehyde was quenched with 50 mM glycine. Cells were then blocked for 20 minutes in either
498 5% normal swine serum (NSS) or 5% NSS with 0.1% saponin (for measurement of total GLUT4 levels).
499 After blocking cells were washed and incubated with anti-HA antibody (Convance, 1:200 in 5% NSS)
500 for 45 minutes before incubation with secondary antibody for 20 minutes. Total and plasma
501 membrane GLUT4-HA was determined by fluorescence plate reader at 485/520 nm. GLUT4
502 translocation was calculated as % of total GLUT4 at the plasma membrane. For palmitate induced
503 insulin resistance assays myotubes were incubated in αMEM overnight supplemented with either 125
504 µM palmitic acid conjugated to BSA or equivalent BSA as a vehicle control before performing assay as
505 above. For assessment of the Prestwick library of compounds, each compound was dissolved in DMSO
506 and added for 1 hour at a final concentration of 10 µM (0.2% DMSO) prior to experimentation.
507 Biological significance for each assay was defined as 50% of control. For basal agonists this was > 50%
508 of 100 nM insulin, for insulin sensitisers this was > 50% of the difference between 1 and 100 nM insulin,
509 and for insulin resistance reversers this was > 50% of the difference between 100 nM insulin and 100
510 nM insulin + palmitate.

511

512 2-deoxyglucose uptake

513 2-deoxyglucose uptake into GLUT4-HA-L6 cells was performed as previously described with
514 modifications (101, 102). Cells were incubated overnight in either αMEM overnight supplemented
515 with either BSA-coupled 125 µM palmitic acid or BSA vehicle control before being washed 3x with
516 HEPES buffed saline (HBS). Cells were then incubated in HBS supplemented with 10 µM unlabelled 2-
517 deoxyglucose and 0.5 µCi/ml [^{3}H]-2-deoxyglucose at 37°C for 5 minutes. Cells were then washed 5x
518 with ice-cold PBS and lysed in 1M NaOH. For non-specific background uptake, 1 well per condition was
519 pre-treated with cytochalasin B. Counts were determined by Perkin Elmer Quantulus GCT Liquid
520 Scintillation Counter (Perkin Elmer, Waltham, MA, USA). Glucose uptake was expressed relatively to

521 protein concentration as determined by bicinchoninic acid (BCA) assay after subtraction of non-
522 specific uptake.

523

524 Ex vivo glucose uptake

525 Ex vivo glucose uptake was performed as previously described (4). Mice were euthanized by cervical
526 dislocation prior to rapid dissection of soleus (C57Bl/6J and BXH9/TyJ) and extensor digitorum longus
527 (EDL) muscle (BXH9/TyJ only). Muscle selection was based on our prior observations that only soleus
528 muscles in C57Bl/6J mice develop diet-induced insulin resistance. Both the soleus and EDL muscles
529 were mounted and then incubated for 1 h in Krebs Henseleit buffer (KHB; 5.5 mM glucose, 2 mM
530 pyruvate and 0.1% BSA) that had been gassed with carbogen (95% O2/5% CO2) supplemented with
531 either 10 µM thiostrepton or a DMSO vehicle control. Glucose uptake was assessed by then switching
532 the muscle into KHB supplemented with 0.375 mCi/ml [3H]-2-dexoyglucose (2-DG), 0.05 mCi/ml [14C]-
533 Mannitol, 100 nM insulin and either thiostrepton (10 µM) or DMSO vehicle control for 20 minutes at
534 30 °C followed by washing in ice-cold PBS and then snap frozen in liquid nitrogen. Samples were lysed
535 in 250 mM NaOH at 70 °C. Tracer in the muscle tissue lysates was quantified by liquid scintillation
536 counting and [3H]-2-DG was corrected for extracellular [14C]-mannitol then normalized to wet weight
537 of the tissue.

538

539 Immunoblotting

540 Glut4-HA-L6 myotubes were incubated overnight in 125 µM palmitate or BSA control prior to
541 treatment with drugs/insulin as indicated. Cells were then washed in ice-cold PBS and lysed by
542 scraping directly into 55 °C Laemmli sample buffer with 10 % (tris 2-carboxyethyl phosphine; TCEP).
543 Samples were then sonicated for 24 s (3s on/3s off) and heated at 65 °C for 5 minutes. SDS-PAGE was
544 performed. Samples were resolved by SDS-PAGE as previously described (4), transferred onto PVDF

545 membranes and blocked in TBS-T (0.1% Tween in Tris-buffered saline) containing 5% skim milk for 1
546 hour. Membranes were then washed 3 x 10 minutes in TBS-T and incubated overnight in primary
547 antibodies against phosphorylated Akt T308 (Cell Signaling Technologies #2965; diluted 1:1000),
548 phosphorylated Akt S473 (Cell Signaling Technologies #9271; diluted 1:1000), pan-Akt (Cell Signaling
549 Technologies #9272; diluted 1:1000), phosphorylated GSK-3α/β S21/9 (Cell Signaling Technologies
550 #9327; diluted 1:1000), GSK3α/β (Cell Signaling Technologies #5676; diluted 1:1000), phosphorylated
551 PRAS40 T246 (Cell Signaling Technologies #13175; diluted 1:1000), PRAS40 (Cell Signaling
552 Technologies #2691; diluted 1:1000), phosphorylated AMPK (Cell Signaling Technologies, #2531;
553 diluated 1:1000), α-tubulin (Cell Signalling Technologies #2125; diluted 1:1000), 14-3-3 (Santa Cruz
554 #sc-1657; diluted 1:5000) . The following day membranes were washed 3 x 10 minutes in TBS-T and
555 incubated for 1 hour in species-appropriate fluorescent or HRP secondary antibodies. Imaging and
556 densitometry were performed using LI-COR Image Studio or a Bio-Rad ChemiDoc Imaging System (Bio-
557 Rad, Hercules, CA, USA) and Image J (103). Phosphorylated proteins were normalised against their
558 relevant controls and data was normalised based on average band intensity.

559

560 Mitochondrial stress test

561 Cellular respirometry (oxygen consumption rate, OCR) was performed using Seahorse XFp miniplates
562 and a Seahorse XF HS Mini Analyzer (Seahorse Bioscience, Copenhagen, Denmark) as previously
563 described (104). GLUT4-HA-L6 myotubes were incubated overnight in either palmitate or BSA control
564 αMEM before treatment with either thiostrepton (10 µM) or DMSO vehicle control. Cells were washed
565 twice with KRBH and incubated in KRBH supplemented with 2.8 mM glucose, thiostrepton or vehicle
566 control without BSA (150 µl/well) at 37°C for 1h in non-CO2 incubator. Cells were then assayed in XFp
567 Analyzer. The OCR was measured after a 12-min equilibration period followed by 3/0/3 min of
568 mix/wait/read cycles. Following stabilization of baseline rates, compounds were injected sequentially
569 to reach a final concentration of: 20 mM glucose, oligomycin (5µg/ml), FCCP (1 µM) and

570 rotenone/antimycin A (5 µM) to assess glucose-dependent respiration (calculated by baseline –
571 glucose OCR), ATP-linked respiration (determined by glucose – oligomycin OCR), maximal respiration
572 (calculated by FCCP – AntA/Rot OCR) and non-mitochondrial respiration respectively (equal to
573 AntA/Rot OCR). Data were normalised against protein concentration and presented as baseline
574 adjusted.

575

576 Acknowledgements

577 We'd like to thank the Sydney Mass Spectrometry facility in the Charles Perkins Centre at the
578 University of Sydney for mass spectrometry support. We'd also like to thank Large Animal Services in
579 the Charles Perkins Centre at The University of Sydney for mouse housing support, and Cordula
580 Hohnen-Behrens, Nicky Konstantopoulos and Briana Spolding for *in vitro* GLUT4 translocation assay
581 assistance.

582

583 1. Bryant NJ, Govers R, James DE. Regulated transport of the glucose transporter GLUT4. Nat Rev
584 Mol Cell Biol. 2002;3(4):267-77.
585 2. James DE, Stockli J, Birnbaum MJ. The aetiology and molecular landscape of insulin resistance.
586 Nat Rev Mol Cell Biol. 2021;22(11):751-71.
587 3. Lotta LA, Gulati P, Day FR, Payne F, Ongen H, van de Bunt M, et al. Integrative genomic analysis
588 implicates limited peripheral adipose storage capacity in the pathogenesis of human insulin resistance.
589 Nat Genet. 2017;49(1):17-26.
590 4. Nelson ME, Madsen S, Cooke KC, Fritzen AM, Thorius IH, Masson SW, et al. Systems-level
591 analysis of insulin action in mouse strains provides insight into tissue-and pathway-specific
592 interactions that drive insulin resistance. Cell Metab. 2022.
593 5. Parks BW, Sallam T, Mehrabian M, Psychogios N, Hui ST, Norheim F, et al. Genetic architecture
594 of insulin resistance in the mouse. Cell Metab. 2015;21(2):334-47.
595 6. Williams EG, Wu Y, Jha P, Dubuis S, Blattmann P, Argmann CA, et al. Systems proteomics of
596 liver mitochondria function. Science. 2016;352(6291):aad0189.
597 7. Yang CH, Mangiafico SP, Waibel M, Loudovaris T, Loh K, Thomas HE, et al. E2f8 and Dlg2 genes
598 have independent effects on impaired insulin secretion associated with hyperglycaemia. Diabetologia.
599 2020;63(7):1333-48.
600 8. Ghazalpour A, Rau CD, Farber CR, Bennett BJ, Orozco LD, van Nas A, et al. Hybrid mouse
601 diversity panel: a panel of inbred mouse strains suitable for analysis of complex genetic traits. Mamm
602 Genome. 2012;23(9-10):680-92.
603 9. Ashbrook DG, Arends D, Prins P, Mulligan MK, Roy S, Williams EG, et al. A platform for
604 experimental precision medicine: The extended BXD mouse family. Cell Syst. 2021;12(3):235-47.e9.

10. Peirce JL, Lu L, Gu J, Silver LM, Williams RW. A new set of BXD recombinant inbred lines from advanced intercross populations in mice. BMC Genet. 2004;5:7.
11. Consortium CC. The genome architecture of the Collaborative Cross mouse genetic reference population. Genetics. 2012;190(2):389-401.
12. Svenson KL, Gatti DM, Valdar W, Welsh CE, Cheng R, Chesler EJ, et al. High-resolution genetic mapping using the Mouse Diversity outbred population. Genetics. 2012;190(2):437-47.
13. Ferguson B, Handoko HY, Mukhopadhyay P, Chitsazan A, Balmer L, Morahan G, et al. Different genetic mechanisms mediate spontaneous versus UVR-induced malignant melanoma. Elife. 2019;8.
14. Baliga NS, Björkegren JLM, Boeke JD, Boutros M, Crawford NPS, Dudley AM, et al. The State of Systems Genetics in 2017. Cell Systems. 2017;4(1):7-15.
15. Seldin M, Yang X, Lusis AJ. Systems genetics applications in metabolism research. Nature metabolism. 2019;1(11):1038-50.
16. Subramanian A, Narayan R, Corsello SM, Peck DD, Natoli TE, Lu X, et al. A Next Generation Connectivity Map: L1000 Platform and the First 1,000,000 Profiles. Cell. 2017;171(6):1437-52.e17.
17. Uva P, Bosco MC, Eva A, Conte M, Garaventa A, Amoroso L, et al. Connectivity Map Analysis Indicates PI3K/Akt/mTOR Inhibitors as Potential Anti-Hypoxia Drugs in Neuroblastoma. Cancers (Basel). 2021;13(11).
18. Lamb J, Crawford ED, Peck D, Modell JW, Blat IC, Wrobel MJ, et al. The Connectivity Map: using gene-expression signatures to connect small molecules, genes, and disease. Science. 2006;313(5795):1929-35.
19. Lamb J. The Connectivity Map: a new tool for biomedical research. Nat Rev Cancer. 2007;7(1):54-60.
20. Matsuda M, DeFronzo RA. Insulin sensitivity indices obtained from oral glucose tolerance testing: comparison with the euglycemic insulin clamp. Diabetes Care. 1999;22(9):1462-70.
21. Churchill GA, Gatti DM, Munger SC, Svenson KL. The Diversity Outbred mouse population. Mamm Genome. 2012;23(9-10):713-8.
22. DeFronzo RA. Lilly lecture 1987. The triumvirate: beta-cell, muscle, liver. A collusion responsible for NIDDM. Diabetes. 1988;37(6):667-87.
23. Anderson EJ, Lustig ME, Boyle KE, Woodlief TL, Kane DA, Lin C-T, et al. Mitochondrial H2O2 emission and cellular redox state link excess fat intake to insulin resistance in both rodents and humans. The Journal of Clinical Investigation. 2009;119(3):573-81.
24. Rath S, Sharma R, Gupta R, Ast T, Chan C, Durham TJ, et al. MitoCarta3.0: an updated mitochondrial proteome now with sub-organelle localization and pathway annotations. Nucleic Acids Res. 2021;49(D1):D1541-d7.
25. Su Z, Deshpande V, James DE, Stockli J. Tankyrase modulates insulin sensitivity in skeletal muscle cells by regulating the stability of GLUT4 vesicle proteins. J Biol Chem. 2018;293(22):8578-87.
26. Chen Y, Lippincott-Schwartz J. Rab10 delivers GLUT4 storage vesicles to the plasma membrane. Commun Integr Biol. 2013;6(3):e23779.
27. Kawanishi M, Tamori Y, Okazawa H, Araki S, Shinoda H, Kasuga M. Role of SNAP23 in insulin-induced translocation of GLUT4 in 3T3-L1 adipocytes. Mediation of complex formation between syntaxin4 and VAMP2. J Biol Chem. 2000;275(11):8240-7.
28. Chawla B, Hedman AC, Sayedyahossein S, Erdemir HH, Li Z, Sacks DB. Absence of IQGAP1 Protein Leads to Insulin Resistance. J Biol Chem. 2017;292(8):3273-89.
29. Díaz-Ruiz A, Guzmán-Ruiz R, Moreno NR, García-Rios A, Delgado-Casado N, Membrives A, et al. Proteasome Dysfunction Associated to Oxidative Stress and Proteotoxicity in Adipocytes Compromises Insulin Sensitivity in Human Obesity. Antioxidants & redox signaling. 2015;23(7):597-612.
30. Minard AY, Wong MK, Chaudhuri R, Tan SX, Humphrey SJ, Parker BL, et al. Hyperactivation of the Insulin Signaling Pathway Improves Intracellular Proteostasis by Coordinately Up-regulating the Proteostatic Machinery in Adipocytes. J Biol Chem. 2016;291(49):25629-40.

31. Antonescu CN, Díaz M, Femia G, Planas JV, Klip A. Clathrin-dependent and independent endocytosis of glucose transporter 4 (GLUT4) in myoblasts: regulation by mitochondrial uncoupling. Traffic. 2008;9(7):1173-90.
32. Robinson LJ, Pang S, Harris DS, Heuser J, James DE. Translocation of the glucose transporter (GLUT4) to the cell surface in permeabilized 3T3-L1 adipocytes: effects of ATP insulin, and GTP gamma S and localization of GLUT4 to clathrin lattices. J Cell Biol. 1992;117(6):1181-96.
33. Fazakerley DJ, Holman GD, Marley A, James DE, Stöckli J, Coster AC. Kinetic evidence for unique regulation of GLUT4 trafficking by insulin and AMP-activated protein kinase activators in L6 myotubes. J Biol Chem. 2010;285(3):1653-60.
34. Sears DD, Hsiao G, Hsiao A, Yu JG, Courtney CH, Ofrecio JM, et al. Mechanisms of human insulin resistance and thiazolidinedione-mediated insulin sensitization. Proceedings of the National Academy of Sciences of the United States of America. 2009;106(44):18745-50.
35. Gallagher IJ, Scheele C, Keller P, Nielsen AR, Remenyi J, Fischer CP, et al. Integration of microRNA changes in vivo identifies novel molecular features of muscle insulin resistance in type 2 diabetes. Genome Med. 2010;2(2):9.
36. Leng S, Zhang W, Zheng Y, Liberman Z, Rhodes CJ, Eldar-Finkelman H, et al. Glycogen synthase kinase 3 beta mediates high glucose-induced ubiquitination and proteasome degradation of insulin receptor substrate 1. J Endocrinol. 2010;206(2):171-81.
37. Josse AR, Atkinson SA, Tarnopolsky MA, Phillips SM. Increased consumption of dairy foods and protein during diet- and exercise-induced weight loss promotes fat mass loss and lean mass gain in overweight and obese premenopausal women. J Nutr. 2011;141(9):1626-34.
38. Phillips BE, Williams JP, Gustafsson T, Bouchard C, Rankinen T, Knudsen S, et al. Molecular networks of human muscle adaptation to exercise and age. PLoS Genet. 2013;9(3):e1003389.
39. Sood S, Gallagher IJ, Lunnon K, Rullman E, Keohane A, Crossland H, et al. A novel multi-tissue RNA diagnostic of healthy ageing relates to cognitive health status. Genome Biol. 2015;16(1):185.
40. Barberio MD, Huffman KM, Giri M, Hoffman EP, Kraus WE, Hubal MJ. Pyruvate Dehydrogenase Phosphatase Regulatory Gene Expression Correlates with Exercise Training Insulin Sensitivity Changes. Med Sci Sports Exerc. 2016;48(12):2387-97.
41. Espah Borujeni A, Mishler DM, Wang J, Huso W, Salis HM. Automated physics-based design of synthetic riboswitches from diverse RNA aptamers. Nucleic Acids Res. 2016;44(1):1-13.
42. Hangelbroek RW, Fazelzadeh P, Tieland M, Boekschoten MV, Hooiveld GJ, van Duynhoven JP, et al. Expression of protocadherin gamma in skeletal muscle tissue is associated with age and muscle weakness. Journal of cachexia, sarcopenia and muscle. 2016;7(5):604-14.
43. Nakhuda A, Josse AR, Gburcik V, Crossland H, Raymond F, Metairon S, et al. Biomarkers of browning of white adipose tissue and their regulation during exercise- and diet-induced weight loss. Am J Clin Nutr. 2016;104(3):557-65.
44. Phillips BE, Kelly BM, Lilja M, Ponce-González JG, Brogan RJ, Morris DL, et al. A Practical and Time-Efficient High-Intensity Interval Training Program Modifies Cardio-Metabolic Risk Factors in Adults with Risk Factors for Type II Diabetes. Front Endocrinol (Lausanne). 2017;8:229.
45. Timmons JA, Atherton PJ, Larsson O, Sood S, Blokhin IO, Brogan RJ, et al. A coding and non-coding transcriptomic perspective on the genomics of human metabolic disease. Nucleic Acids Research. 2018;46(15):7772-92.
46. Timmons JA, Anighoro A, Brogan RJ, Stahl J, Wahlestedt C, Farquhar DG, et al. A human-based multi-gene signature enables quantitative drug repurposing for metabolic disease. eLife. 2022;11:e68832.
47. Fazakerley DJ, van Gerwen J, Cooke KC, Duan X, Needham EJ, Madsen S, et al. Phosphoproteomics reveals rewiring of the insulin signaling network and multi-nodal defects in insulin resistance. bioRxiv. 2022:2022.05.26.493198.
48. Timmers S, Konings E, Bilet L, Houtkooper RH, van de Weijer T, Goossens GH, et al. Calorie restriction-like effects of 30 days of resveratrol supplementation on energy metabolism and metabolic profile in obese humans. Cell Metab. 2011;14(5):612-22.

49. Knowler WC, Barrett-Connor E, Fowler SE, Hamman RF, Lachin JM, Walker EA, et al. Reduction in the incidence of type 2 diabetes with lifestyle intervention or metformin. N Engl J Med. 2002;346(6):393-403.
50. Geng L, Lam KSL, Xu A. The therapeutic potential of FGF21 in metabolic diseases: from bench to clinic. Nat Rev Endocrinol. 2020;16(11):654-67.
51. Bailly C. The bacterial thiopeptide thiostrepton. An update of its mode of action, pharmacological properties and applications. Eur J Pharmacol. 2022;914:174661.
52. Stöckli J, Davey JR, Hohnen-Behrens C, Xu A, James DE, Ramm G. Regulation of Glucose Transporter 4 Translocation by the Rab Guanosine Triphosphatase-Activating Protein AS160/TBC1D4: Role of Phosphorylation and Membrane Association. Molecular Endocrinology. 2008;22(12):2703-15.
53. Govers R, Coster ACF, James DE. Insulin increases cell surface GLUT4 levels by dose dependently discharging GLUT4 into a cell surface recycling pathway. Mol Cell Biol. 2004;24(14):6456-66.
54. Cho H, Mu J, Kim JK, Thorvaldsen JL, Chu Q, Crenshaw EB, 3rd, et al. Insulin resistance and a diabetes mellitus-like syndrome in mice lacking the protein kinase Akt2 (PKB beta). Science. 2001;292(5522):1728-31.
55. Hoehn KL, Hohnen-Behrens C, Cederberg A, Wu LE, Turner N, Yuasa T, et al. IRS1-independent defects define major nodes of insulin resistance. Cell Metab. 2008;7(5):421-33.
56. Hoy AJ, Brandon AE, Turner N, Watt MJ, Bruce CR, Cooney GJ, et al. Lipid and insulin infusion-induced skeletal muscle insulin resistance is likely due to metabolic feedback and not changes in IRS-1, Akt, or AS160 phosphorylation. Am J Physiol-Endoc M. 2009;297(1):E67-E75.
57. Cameron AR, Logie L, Patel K, Erhardt S, Bacon S, Middleton P, et al. Metformin selectively targets redox control of complex I energy transduction. Redox Biol. 2018;14:187-97.
58. Madiraju AK, Erion DM, Rahimi Y, Zhang XM, Braddock DT, Albright RA, et al. Metformin suppresses gluconeogenesis by inhibiting mitochondrial glycerophosphate dehydrogenase. Nature. 2014;510(7506):542-6.
59. Alexopoulos SJ, Chen S-Y, Brandon AE, Salamoun JM, Byrne FL, Garcia CJ, et al. Mitochondrial uncoupler BAM15 reverses diet-induced obesity and insulin resistance in mice. Nature Communications. 2020;11(1):2397.
60. Zhang L, Ging NC, Komoda T, Hanada T, Suzuki T, Watanabe K. Antibiotic susceptibility of mammalian mitochondrial translation. FEBS Lett. 2005;579(28):6423-7.
61. Weinhaeuser I, Pereira-Martins D, Hilberink JR, Ammatuna E, Huls GA, Rego EM, et al. Functional Drug Screen Identifies Thiostrepton, NAMPT Inhibitors and Metformin As Potential Candidates to Target the Macrophage Tumor Microenvironment in Acute Myeloid Leukemia. Blood. 2022;140(Supplement 1):8793-4.
62. Cunniff B, Newick K, Nelson KJ, Wozniak AN, Beuschel S, Leavitt B, et al. Disabling Mitochondrial Peroxide Metabolism via Combinatorial Targeting of Peroxiredoxin 3 as an Effective Therapeutic Approach for Malignant Mesothelioma. PLOS ONE. 2015;10(5):e0127310.
63. Hoehn KL, Salmon AB, Hohnen-Behrens C, Turner N, Hoy AJ, Maghzal GJ, et al. Insulin resistance is a cellular antioxidant defense mechanism. Proceedings of the National Academy of Sciences of the United States of America. 2009;106(42):17787-92.
64. Herzig S, Shaw RJ. AMPK: guardian of metabolism and mitochondrial homeostasis. Nat Rev Mol Cell Biol. 2018;19(2):121-35.
65. Richter EA, Hargreaves M. Exercise, GLUT4, and skeletal muscle glucose uptake. Physiol Rev. 2013;93(3):993-1017.
66. Jensen TE, Schjerling P, Viollet B, Wojtaszewski JF, Richter EA. AMPK α1 activation is required for stimulation of glucose uptake by twitch contraction, but not by H2O2, in mouse skeletal muscle. PloS one. 2008;3(5).
67. Göransson O, McBride A, Hawley SA, Ross FA, Shpiro N, Foretz M, et al. Mechanism of action of A-769662, a valuable tool for activation of AMP-activated protein kinase. J Biol Chem. 2007;282(45):32549-60.

757 68. Guo Q, Xu Z, Zhou D, Fu T, Wang W, Sun W, et al. Mitochondrial proteostasis stress in muscle
758 drives a long-range protective response to alleviate dietary obesity independently of ATF4. Sci Adv.
759 2022;8(30):eabo0340.
760 69. Hall C, Yu H, Choi E. Insulin receptor endocytosis in the pathophysiology of insulin resistance.
761 Exp Mol Med. 2020;52(6):911-20.
762 70. Lee J, Kim MS. The role of GSK3 in glucose homeostasis and the development of insulin
763 resistance. Diabetes Res Clin Pract. 2007;77 Suppl 1:S49-57.
764 71. Bernier M, Harney D, Koay YC, Diaz A, Singh A, Wahl D, et al. Elucidating the mechanisms by
765 which disulfiram protects against obesity and metabolic syndrome. npj Aging and Mechanisms of
766 Disease. 2020;6(1):8.
767 72. Bernier M, Mitchell SJ, Wahl D, Diaz A, Singh A, Seo W, et al. Disulfiram Treatment Normalizes
768 Body Weight in Obese Mice. Cell Metab. 2020;32(2):203-14.e4.
769 73. Gong L, Guo S, Zou Z. Resveratrol ameliorates metabolic disorders and insulin resistance in
770 high-fat diet-fed mice. Life Sci. 2020;242:117212.
771 74. Shu L, Hou G, Zhao H, Huang W, Song G, Ma H. Resveratrol improves high-fat diet-induced
772 insulin resistance in mice by downregulating the lncRNA NONMMUT008655.2. American journal of
773 translational research. 2020;12(1):1-18.
774 75. Rosales-Soto G, Diaz-Vegas A, Casas M, Contreras-Ferrat A, Jaimovich E. Fibroblast growth
775 factor-21 potentiates glucose transport in skeletal muscle fibers. Journal of Molecular Endocrinology.
776 2020;65(3):85-95.
777 76. Oost LJ, Kustermann M, Armani A, Blaauw B, Romanello V. Fibroblast growth factor 21
778 controls mitophagy and muscle mass. Journal of cachexia, sarcopenia and muscle. 2019;10(3):630-42.
779 77. Maier T, Güell M, Serrano L. Correlation of mRNA and protein in complex biological samples.
780 FEBS Lett. 2009;583(24):3966-73.
781 78. de Sousa Abreu R, Penalva LO, Marcotte EM, Vogel C. Global signatures of protein and mRNA
782 expression levels. Mol Biosyst. 2009;5(12):1512-26.
783 79. Gatti DM, Svenson KL, Shabalin A, Wu L-Y, Valdar W, Simecek P, et al. Quantitative Trait Locus
784 Mapping Methods for Diversity Outbred Mice. G3 Genes|Genomes|Genetics. 2014;4(9):1623-33.
785 80. Cavalli V, Vilbois F, Corti M, Marcote MJ, Tamura K, Karin M, et al. The stress-induced MAP
786 kinase p38 regulates endocytic trafficking via the GDI:Rab5 complex. Mol Cell. 2001;7(2):421-32.
787 81. Thompson JA, Carlson GM. The regulatory α and β subunits of phosphorylase kinase directly
788 interact with its substrate, glycogen phosphorylase. Biochem Biophys Res Commun. 2017;482(2):221-
789 5.
790 82. Polishchuk SV, Brandt NR, Meyer HE, Varsányi M, Heilmeyer LM, Jr. Does phosphorylase
791 kinase control glycogen biosynthesis in skeletal muscle? FEBS Lett. 1995;362(3):271-5.
792 83. Ding VW, Chen R-H, McCormick F. Differential regulation of glycogen synthase kinase 3β by
793 insulin and Wnt signaling. J Biol Chem. 2000;275(42):32475-81.
794 84. Skurat AV, Dietrich AD, Roach PJ. Interaction between glycogenin and glycogen synthase. Arch
795 Biochem Biophys. 2006;456(1):93-7.
796 85. Trefely S, Khoo PS, Krycer JR, Chaudhuri R, Fazakerley DJ, Parker BL, et al. Kinome Screen
797 Identifies PFKFB3 and Glucose Metabolism as Important Regulators of the Insulin/Insulin-like Growth
798 Factor (IGF)-1 Signaling Pathway. J Biol Chem. 2015;290(43):25834-46.
799 86. Newick K, Cunniff B, Preston K, Held P, Arbiser J, Pass H, et al. Peroxiredoxin 3 is a redox-
800 dependent target of thiostrepton in malignant mesothelioma cells. PLoS One. 2012;7(6):e39404.
801 87. Liu J, Wen D, Fang X, Wang X, Liu T, Zhu J. p38MAPK Signaling Enhances Glycolysis Through
802 the Up-Regulation of the Glucose Transporter GLUT-4 in Gastric Cancer Cells. Cell Physiol Biochem.
803 2015;36(1):155-65.
804 88. Kulisz A, Chen N, Chandel NS, Shao Z, Schumacker PT. Mitochondrial ROS initiate
805 phosphorylation of p38 MAP kinase during hypoxia in cardiomyocytes. Am J Physiol Lung Cell Mol
806 Physiol. 2002;282(6):L1324-9.

807 89. Wang F, Qi XM, Wertz R, Mortensen M, Hagen C, Evans J, et al. p38γ MAPK Is Essential for
808 Aerobic Glycolysis and Pancreatic Tumorigenesis. Cancer Res. 2020;80(16):3251-64.
809 90. Chesler EJ, Gatti DM, Morgan AP, Strobel M, Trepanier L, Oberbeck D, et al. Diversity Outbred
810 Mice at 21: Maintaining Allelic Variation in the Face of Selection. G3 (Bethesda, Md). 2016;6(12):3893-
811 902.
812 91. Morgan AP, Fu CP, Kao CY, Welsh CE, Didion JP, Yadgary L, et al. The Mouse Universal
813 Genotyping Array: From Substrains to Subspecies. G3 (Bethesda, Md). 2015;6(2):263-79.
814 92. Broman KW, Gatti DM, Svenson KL, Sen Ś, Churchill GA. Cleaning Genotype Data from Diversity
815 Outbred Mice. G3 Genes|Genomes|Genetics. 2019;9(5):1571-9.
816 93. Rappsilber J, Mann M, Ishihama Y. Protocol for micro-purification, enrichment, pre-
817 fractionation and storage of peptides for proteomics using StageTips. Nat Protoc. 2007;2(8):1896-906.
818 94. Demichev V, Messner CB, Vernardis SI, Lilley KS, Ralser M. DIA-NN: neural networks and
819 interference correction enable deep proteome coverage in high throughput. Nat Methods.
820 2020;17(1):41-4.
821 95. R Core Team R. R: A language and environment for statistical computing. 2013.
822 96. Dabney A, Storey JD, Warnes GJRpv. qvalue: Q-value estimation for false discovery rate
823 control. 2010;1(0).
824 97. Yu G, Wang L-G, Han Y, He Q-YJOajoib. clusterProfiler: an R package for comparing biological
825 themes among gene clusters. 2012;16(5):284-7.
826 98. Liao Y, Wang J, Jaehnig EJ, Shi Z, Zhang B. WebGestalt 2019: gene set analysis toolkit with
827 revamped UIs and APIs. Nucleic Acids Res. 2019;47(W1):W199-w205.
828 99. Broman KW, Gatti DM, Simecek P, Furlotte NA, Prins P, Sen Ś, et al. R/qtl2: Software for
829 Mapping Quantitative Trait Loci with High-Dimensional Data and Multiparent Populations. Genetics.
830 2019;211(2):495-502.
831 100. Stegle O, Parts L, Piipari M, Winn J, Durbin R. Using probabilistic estimation of expression
832 residuals (PEER) to obtain increased power and interpretability of gene expression analyses. Nat
833 Protoc. 2012;7(3):500-7.
834 101. Carey AL, Steinberg GR, Macaulay SL, Thomas WG, Holmes AG, Ramm G, et al. Interleukin-6
835 increases insulin-stimulated glucose disposal in humans and glucose uptake and fatty acid oxidation
836 in vitro via AMP-activated protein kinase. Diabetes. 2006;55(10):2688-97.
837 102. Masson SWC, Sorrenson B, Shepherd PR, Merry TL. beta-catenin regulates muscle glucose
838 transport via actin remodelling and M-cadherin binding. Mol Metab. 2020;42:101091.
839 103. Schneider CA, Rasband WS, Eliceiri KW. NIH Image to ImageJ: 25 years of image analysis. Nat
840 Methods. 2012;9(7):671-5.
841 104. Yau B, Naghiloo S, Diaz-Vegas A, Carr AV, Van Gerwen J, Needham EJ, et al. Proteomic
842 pathways to metabolic disease and type 2 diabetes in the pancreatic islet. iScience.
843 2021;24(10):103099.

844

845

846 Figure Legends

847 Figure 1. Metabolic and proteomic diversity of Diversity Outbred in Oz (DOz) mice. (A) Schematic of
848 metabolic phenotyping and quadricep proteomics in chow fed DOz mice. (B) Blood glucose and insulin
849 levels during a GTT. (C) Whole-body insulin sensitivity (Matsuda Index, formula shown above) and
850 adiposity of DOz mice (n= 215). (D) Comparison of coefficient of variation (CV) of insulin of Matsuda
851 Index across inbred strains and diets versus chow fed DOz mice. (E) Relative enrichment of
852 mitochondrial (Mito) proteins in mitochondrial fraction and post-mitochondrial fraction (PMF) of
853 quadricep proteomes. (F) Relative protein CV across mitochondrial and post-mitochondrial quadricep
854 fractions. (G) Biological pathways enriched in mitochondrial and post-mitochondrial quadricep
855 fractions, running enrichment score for a given pathway (ES) on y-axis and proteins ranked by CV on
856 x-axis. Significance testing was performed by Chi-square test. * Indicates a significant difference $P <$
857 0.01.

858

859 Figure 2. Linear modelling of quadricep proteome and whole-body insulin sensitivity. (A-B) Volcano
860 plot with Matsuda Index effect sizes (x-axis) and significance (y-axis) for mitochondrial (A) and post-
861 mitochondrial (B) quadricep proteins using a linear model with adiposity as a covariate. Significant
862 proteins with positive and negative effect sizes are indicated in red and blue, respectively. (C)
863 Comparison of positively and negatively associated proteins between fractions. (D) Number of
864 proteins identified in each fraction with known roles in insulin or AMPK signalling. (E-F) Volcano plot
865 shown in A with mitochondrial (E) and post-mitochondrial fraction (F) proteins shown in black that
866 have documented roles in indicated signalling pathways. Adjusted p-value threshold is indicated (red
867 dotted line). (G) Pathways enriched for proteins which positively and negative associate with Matsuda
868 Index. Effect sizes of proteins within a given pathway and running enrichment score (ES) for a that
869 pathway on y-axis and proteins ranked by CV on x-axis. (ES) on y-axis and proteins ranked by CV on x-
870 axis. of proteins within pathways that are enriched for proteins associated with whole-body insulin

871 sensitivity. Proteins ranked by Matsuda Index effect size on x-axis. Linear modelling was performed
872 using a gaussian distribution with q-value adjustment of p-values. Enrichment tests between fractions
873 were performed by Chi-square test. * Indicates a significant difference $P < 0.01$.

874

875 Figure 3. Integration of proteomic data via Connectivity Map. (A-B) Workflow includes filtering for
876 proteins with pQTL (A) and negative association with Matsuda Index (B) prior to Connectivity Map
877 query. (A) Example of whole-genome genetic scans with pQTL presence or absence. (B) Left side of
878 volcano plots from Figure 2A-B (proteins negatively associated with Matsuda Index) is shown with
879 proteins comprised in Molecular Fingerprint of insulin resistance (IR) indicated in black. Proteins with
880 human homologues are highlighted that. (C) Top 10 KEGG pathways enriched in the molecular
881 fingerprint of insulin resistance with proteins of interest highlighted. (D) Distribution of Connectivity
882 Map (CMAP) scores for identified small molecules and ligands with compounds of interest indicated.

883

884 Figure 4. Prestwick library of FDA-approved drugs that modulate GLUT4 translocation in L6 myotubes.
885 (A) Schematic representation of the three assays performed. (B) Small molecules that promote GLUT4
886 exocytosis to the plasma membrane independently of insulin with controls (Basal, Insulin) on the left.
887 (C) Small molecules that potentiate a submaximal dose of insulin (1 nM) with controls (Basal, 1 nM
888 and 100 nM Insulin) on the left. Compounds were added in combination with 1 nM insulin. (D) Small
889 molecules that reverse palmitate induced insulin resistance with controls (Basal, Insulin, Insulin +
890 Palmitate) on the left. Compounds were added in combination with 100 nM insulin following palmitate
891 treatment. (E) Venn diagram of compound overlap between assays. Biological significance for each
892 assay was defined as 50% of corresponding control, see methods for details. Plasma-membrane; PM.

893

894 Figure 5. Cross-validation of Connectivity Map and Prestwick library. (A) Scoring matrix of top 20
895 scoring compounds present in both Connectivity Map (CMAP) and the Prestwick library screens (Basal
896 Agonists, Bas.Ag.; Insulin Sensitizer, Ins. Sens; Insulin Resistance Reversers, Ins. Res. Rev). (B-C) Insulin
897 stimulated GLUT4 translocation to the plasma membrane (PM, B) and 2-deoxyglucose uptake (C) in
898 control and insulin resistant L6 myotubes (Palmitate) treated with thiostrepton or vehicle control. (D)
899 Insulin stimulated 2-deoxyglucose uptake in soleus and extensor digitorum longus (EDL) muscles from
900 chow and WD fed C57BL/6J and BXH9/TyJ following ex vivo treatment with thiostrepton or vehicle
901 control. Data are mean with individual data points shown, n=3-4 (B-C), n=3-5 (BXH9) n=11-14
902 (C57BL/6J). Significance was determined by one-way ANOVA with Student's post hoc test. ** Indicates
903 significant difference from control (Basal or chow fed C57BL6/J) group ($p < 0.01$), * Indicates significant
904 difference from control ($p < 0.05$). # Indicates significant difference from palmitate-treated or WD-fed
905 fed control group ($p < 0.05$).

906

907 Figure 6. Effect of thiostrepton on insulin signalling. (A-E) Immunoblotting with indicated antibodies
908 of control and palmitate treated GLUT4-HA-L6 myotubes following treatment with thiostrepton or
909 vehicle control and stimulation with 0, 1, or 10 nM insulin. (A) Representative immunoblot shown of
910 3 independent experiments. (B-E) Quantification of immunoblots in A, Akt S473 (B), Akt T308 (C),
911 GSK3β S9 (D) and PRAS40 T246 (E). Data are mean with individual data points, n=3. Significance was
912 determined by two-way ANOVA with Student's post hoc test. * Indicates a significant effect of insulin
913 $P < 0.01$.

914

915 Figure 7. Effect of thiostrepton on mitochondrial respiration and glycolysis. (A-B) Oxygen consumption
916 rates (A) and extracellular acidification rates (B) in control and palmitate treated GLUT4-HA-L6
917 myotubes treated with either thiostrepton or vehicle control. (C) Immunoblotting of AMPK signalling
918 in control and palmitate treated (Palm.) GLUT4-HA-L6 myotubes treated with either thiostrepton

919 (Thio.), vehicle control (Bas.) or positive control A-769662 (A76.). Representative immunoblots shown
920 of 3 independent experiments. (D-E) Quantification of immunoblots in C, AMPK T172 (D) and ACC S79
921 (E) phosphorylation following thiostrepton or A-769662 treatment. Data are mean with individual data
922 points shown, n=3. * Indicates significant difference from control cells, # indicates significant
923 difference from palmitate treated cells $p < 0.05$.

924

925 Supplementary Figure 1. Comparison of linear modelling approaches for DOz insulin sensitivity and
926 muscle proteomics. (A-B) Volcano plot with Matsuda Index effect sizes (x-axis) and significance (y-axis)
927 for mitochondrial (A) and post-mitochondrial fraction (B) proteins. (C-D) Mitochondrial (C) and post-
928 mitochondrial fraction (D) negative log10 p-values for Matsuda Index effect sizes from linear models
929 with and without adiposity as a covariate. Dashed red line indicates FDR adjusted $p < 0.05$.

930

931 Supplementary Figure 2. Evaluation of Connectivity Map analysis. (A) Raw Connectivity Map (CMAP)
932 scores for compounds and ligands identified by Connectivity map using either a pQTL filtered signature
933 (Fingerprint) or a signature of the 150 proteins with the largest negative effect sizes. (B) Comparison
934 of z scored GLUT4 at plasma membrane (PM) after treatment with Prestwick library compounds based
935 on CMAP significance. Data are mean with individual data points. Significance was determined by two-
936 way ANOVA with Student's post hoc test. * Indicates a significant difference between groups $P < 0.01$.

937

938 Supplementary Figure 3. Effect of western diet feeding on C57BL/6J and BxH9/TyJ mice body
939 composition and insulin sensitivity. (A-E) Body weights (A), adiposity (B), blood glucose (C) and insulin
940 (D) during a glucose tolerance test, and Matsuda Index (E) of C57BL/6J and BxH9/TyJ mice fed a chow
941 of high-fat/high-sugar (western diet; WD) for 8 weeks. Data are mean with individual data points, n=
942 4-6 (BxH9), n=15 (C57BL/6J).

943 Supplementary Table 1. List of proteins and their Matsuda Index effect sizes which comprise our pQTL-

944 filtered molecular fingerprint of insulin resistance.

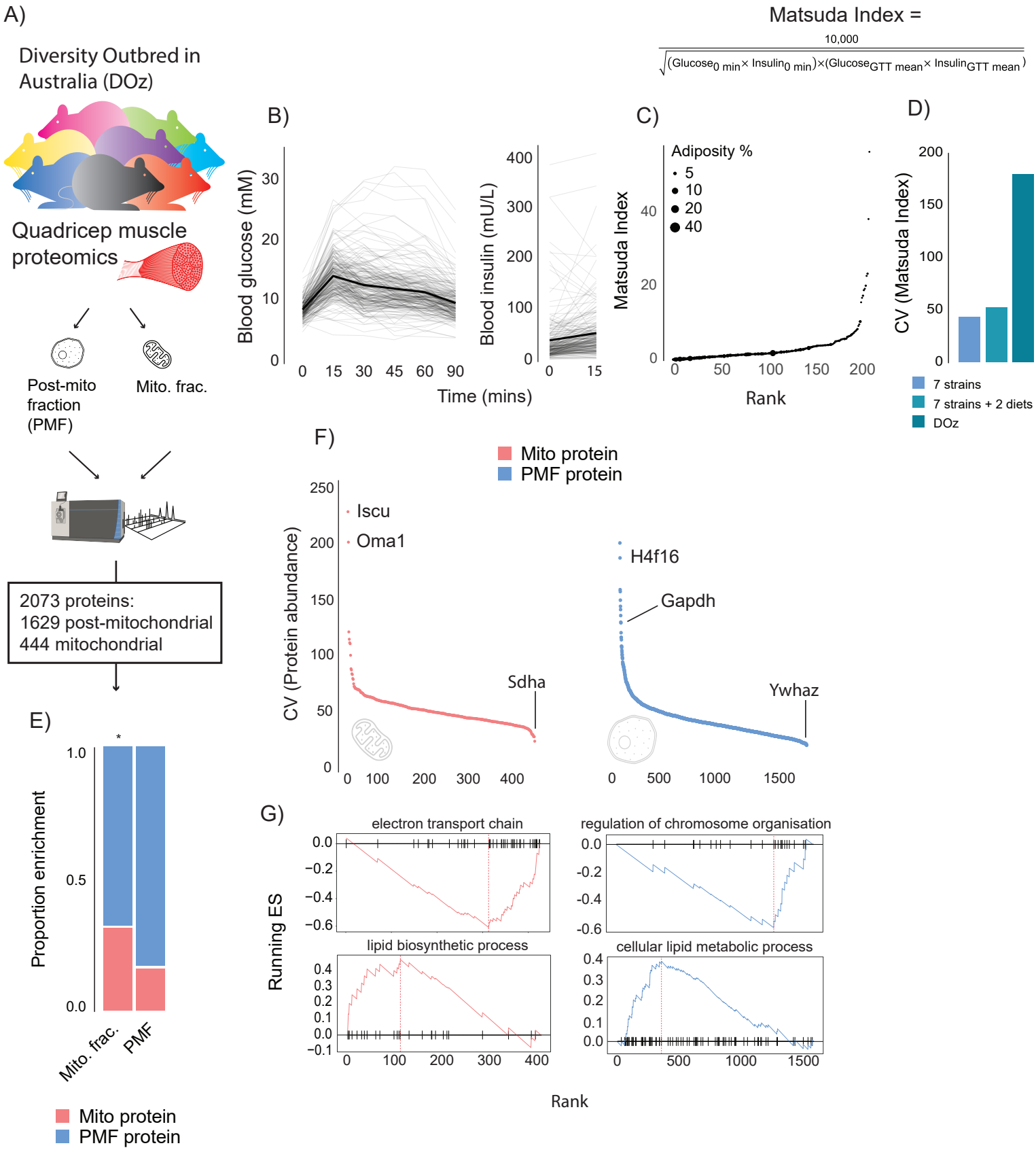
A)
Matsuda Index =
10,000
√((Glucose0 min× Insulin0 min)×(GlucoseGTT mean× InsulinGTT mean))
Diversity Outbred in Australia (DOz)
Quadricep muscle proteomics
Post-mito fraction (PMF)
Mito. frac.
2073 proteins:
1629 post-mitochondrial
444 mitochondrial
B)
Blood glucose (mM)
Time (mins)
Blood insulin (mU/L)
C)
Matsuda Index
Adiposity %
5
10
20
40
Rank
D)
CV (Matsuda Index)
7 strains
7 strains + 2 diets
DOz
E)
Proportion enrichment
Mito. frac.
PMF
Mito protein
PMF protein
F)
Mito protein
PMF protein
CV (Protein abundance)
Iscu
Oma1
Sdha
H4f16
Gapdh
Ywhaz
G)
Running ES
electron transport chain
regulation of chromosome organisation
lipid biosynthetic process
cellular lipid metabolic process
Rank

Figure 2

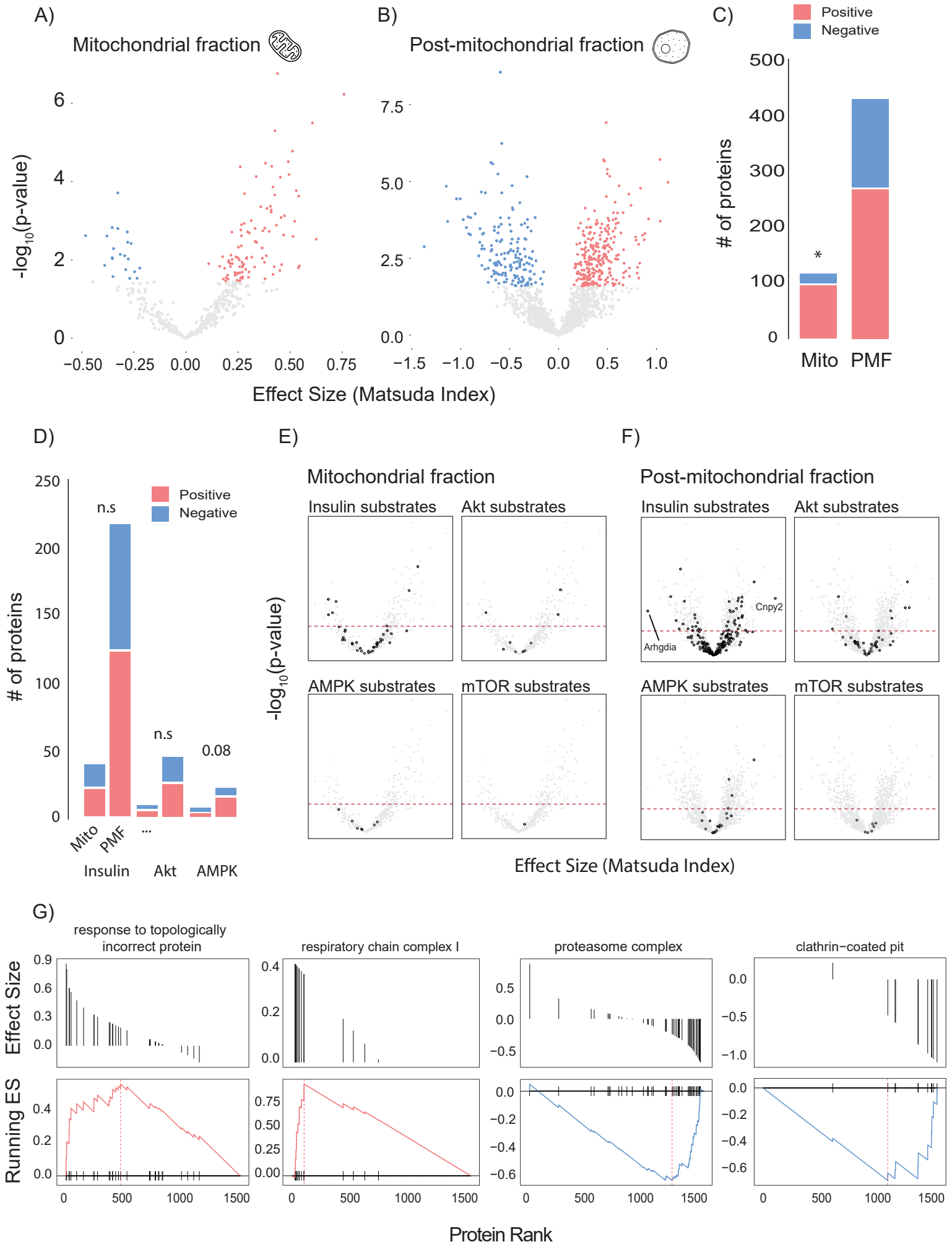
A)
Mitochondrial fraction
B)
Post-mitochondrial fraction
C)
Positive
Negative
-log10(p-value)
Effect Size (Matsuda Index)
# of proteins
Mito
PMF
D)
n.s
n.s
0.08
Insulin
Akt
AMPK
E)
Mitochondrial fraction
F)
Post-mitochondrial fraction
Insulin substrates
Akt substrates
AMPK substrates
mTOR substrates
Cnpy2
Arhgdia
G)
response to topologically incorrect protein
respiratory chain complex I
proteasome complex
clathrin−coated pit
Effect Size
Running ES
Protein Rank

Figure 3:

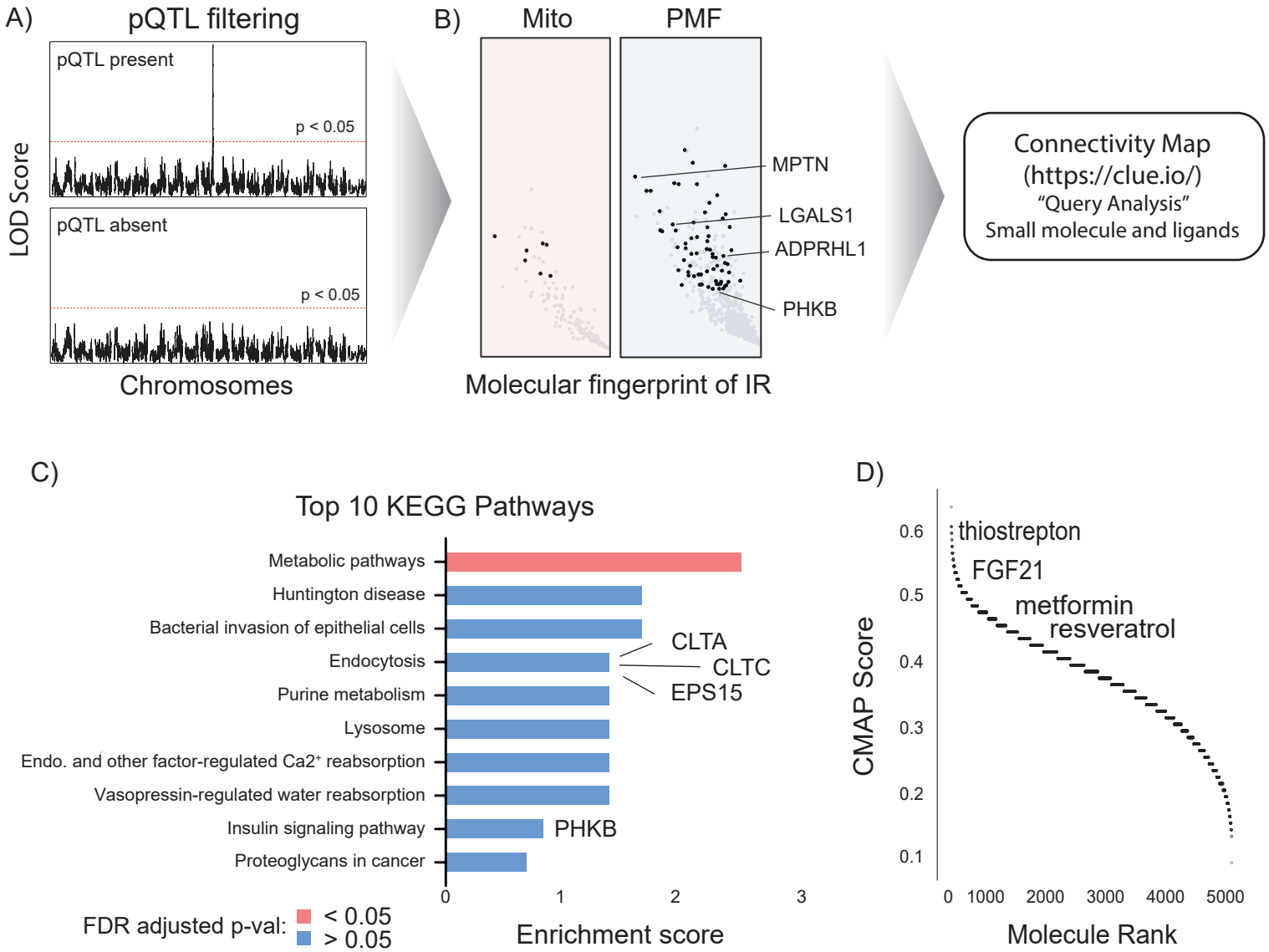
A)
pQTL filtering
pQTL present
p < 0.05
pQTL absent
p < 0.05
LOD Score
Chromosomes
B)
Mito
PMF
MPTN
LGALS1
ADPRHL1
PHKB
Molecular fingerprint of IR
Connectivity Map
(https://clue.io/)
"Query Analysis"
Small molecule and ligands
C)
Top 10 KEGG Pathways
Metabolic pathways
Huntington disease
Bacterial invasion of epithelial cells
Endocytosis
Purine metabolism
Lysosome
Endo. and other factor-regulated Ca2+ reabsorption
Vasopressin-regulated water reabsorption
Insulin signaling pathway
Proteoglycans in cancer
CLTA
CLTC
EPS15
PHKB
0
1
2
3
Enrichment score
FDR adjusted p-val:
< 0.05
> 0.05
D)
CMAP Score
0.6
0.5
0.4
0.3
0.2
0.1
thiostrepton
FGF21
metformin
resveratrol
0
1000
2000
3000
4000
5000
Molecule Rank

Figure 4:

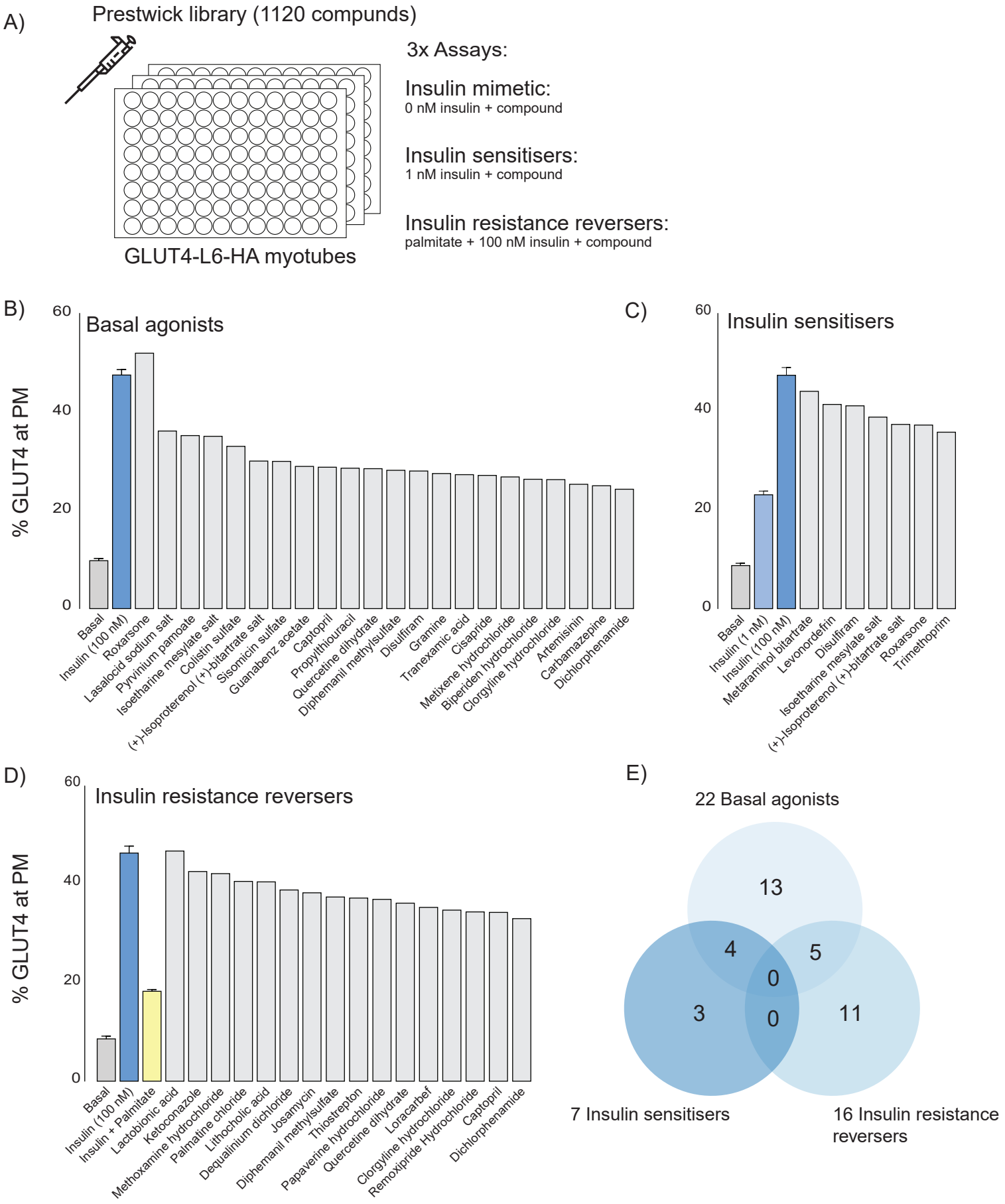
A)
Prestwick library (1120 compunds)
3x Assays:
Insulin mimetic:
0 nM insulin + compound
Insulin sensitisers:
1 nM insulin + compound
Insulin resistance reversers:
palmitate + 100 nM insulin + compound
GLUT4-L6-HA myotubes
B)
Basal agonists
% GLUT4 at PM
60
40
20
0
Basal
Insulin (100 nM)
Roxarsone
Lasalocid sodium salt
Pyrvinium pamoate
Isoetharine mesylate salt
Colistin sulfate
(+)-Isoproterenol (+)-bitartrate salt
Sisomicin sulfate
Guanabenz acetate
Captopril
Propylthiouracil
Quercetine dihydrate
Diphemanil methylsulfate
Disulfiram
Gramine
Tranexamic acid
Cisapride
Metixene hydrochloride
Biperiden hydrochloride
Clorgyline hydrochloride
Artemisinin
Carbamazepine
Dichlorphenamide
C)
Insulin sensitisers
60
40
20
0
Basal
Insulin (1 nM)
Insulin (100 nM)
Metaraminol bitartrate
Levonordefrin
Disulfiram
Isoetharine mesylate salt
(+)-Isoproterenol (+)-bitartrate salt
Roxarsone
Trimethoprim
D)
Insulin resistance reversers
% GLUT4 at PM
60
40
20
0
Basal
Insulin (100 nM)
Insulin + Palmitate
Lactobionic acid
Ketoconazole
Methoxamine hydrochloride
Palmatine chloride
Lithocholic acid
Dequalinium dichloride
Josamycin
Diphemanil methylsulfate
Thiostrepton
Papaverine hydrochloride
Quercetine dihydrate
Loracarbef
Clorgyline hydrochloride
Remoxipride Hydrochloride
Captopril
Dichlorphenamide
E)
22 Basal agonists
13
4
5
0
3
0
11
7 Insulin sensitisers
16 Insulin resistance reversers

Figure 5:

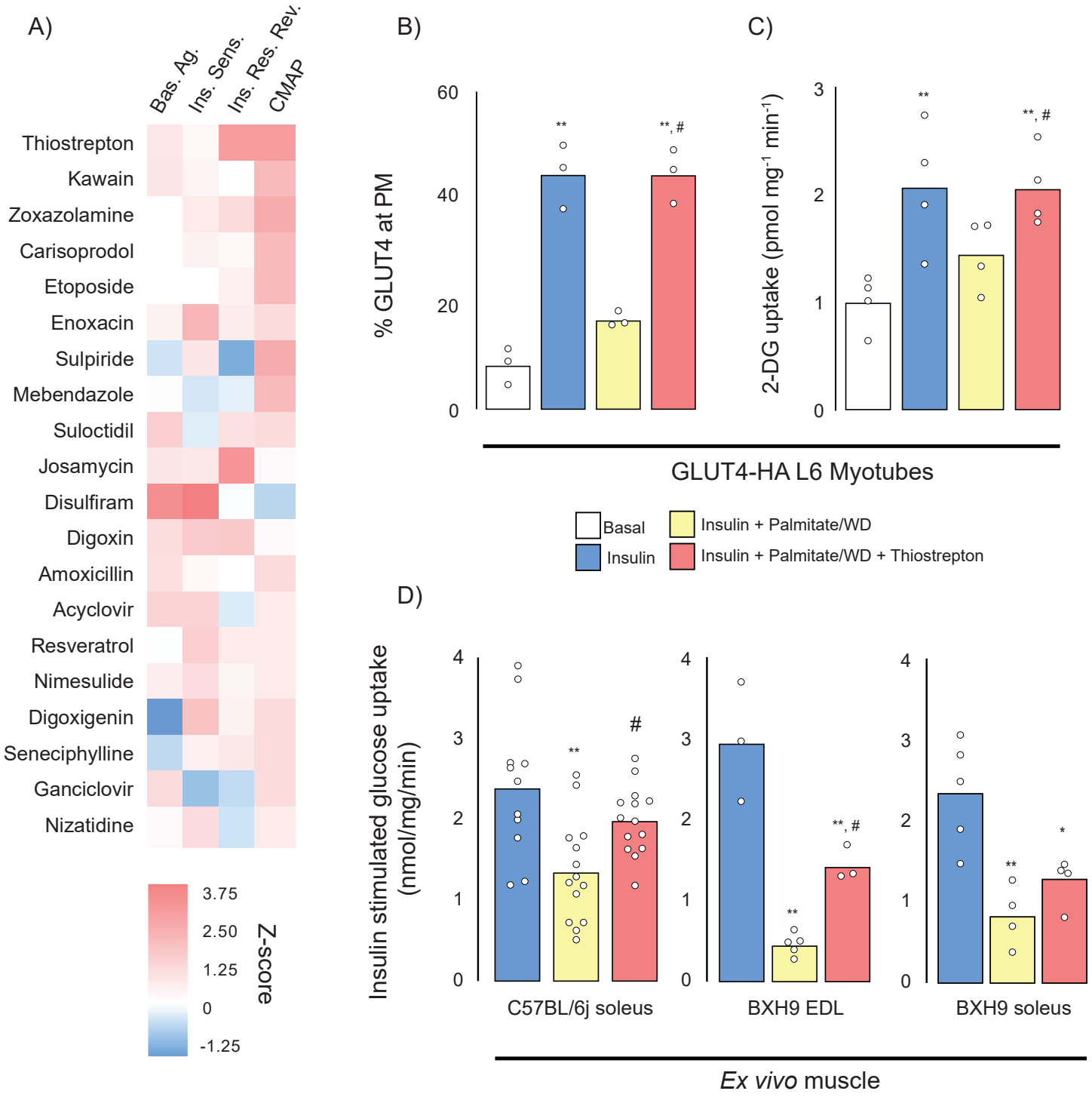
A)
Bas. Ag.
Ins. Sens.
Ins. Res.
Rev. CMAP
Thiostrepton
Kawain
Zoxazolamine
Carisoprodol
Etoposide
Enoxacin
Sulpiride
Mebendazole
Suloctidil
Josamycin
Disulfiram
Digoxin
Amoxicillin
Acyclovir
Resveratrol
Nimesulide
Digoxigenin
Seneciphylline
Ganciclovir
Nizatidine
3.75
2.50
1.25
0
-1.25
Z-score
B)
% GLUT4 at PM
60
40
20
0
**
**, #
C)
2-DG uptake (pmol mg-1 min-1)
3
2
1
0
**
**, #
GLUT4-HA L6 Myotubes
Basal
Insulin
Insulin + Palmitate/WD
Insulin + Palmitate/WD + Thiostrepton
D)
Insulin stimulated glucose uptake (nmol/mg/min)
4
3
2
1
0
**
#
**
**, #
**
*
C57BL/6j soleus
BXH9 EDL
BXH9 soleus
Ex vivo muscle

Figure 6

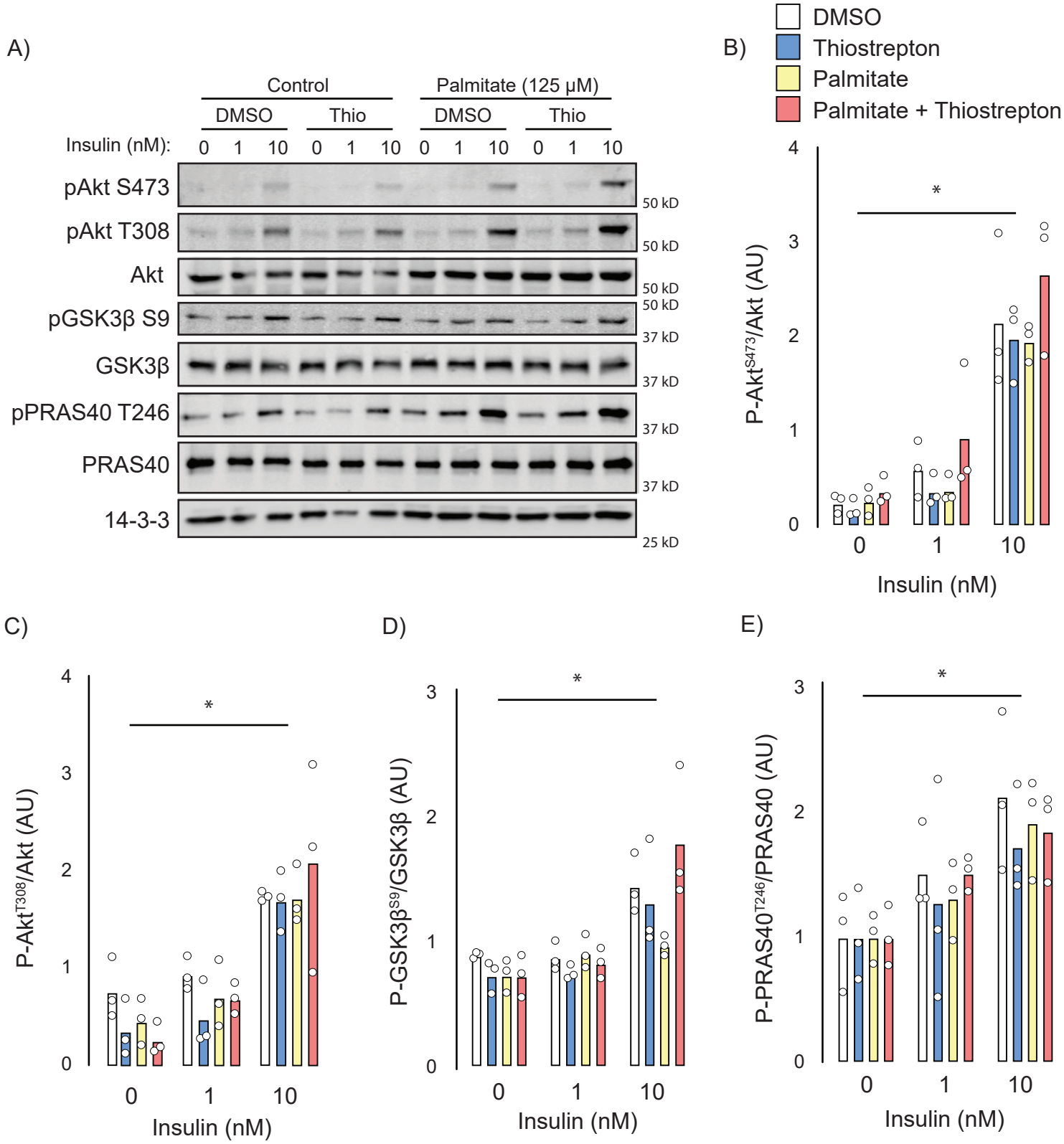
A)
Control
Palmitate (125 μM)
DMSO
Thio
DMSO
Thio
Insulin (nM): 0 1 10 0 1 10 0 1 10 0 1 10
pAkt S473
pAkt T308
Akt
pGSK3β S9
GSK3β
pPRAS40 T246
PRAS40
14-3-3
50 kD
50 kD
50 kD
50 kD
37 kD
37 kD
37 kD
37 kD
25 kD
B)
DMSO
Thiostrepton
Palmitate
Palmitate + Thiostrepton
P-Akt^{S473}/Akt (AU)
Insulin (nM)
C)
P-Akt^{T308}/Akt (AU)
Insulin (nM)
D)
P-GSK3β^{S9}/GSK3β (AU)
Insulin (nM)
E)
P-PRAS40^{T246}/PRAS40 (AU)
Insulin (nM)

Figure 7

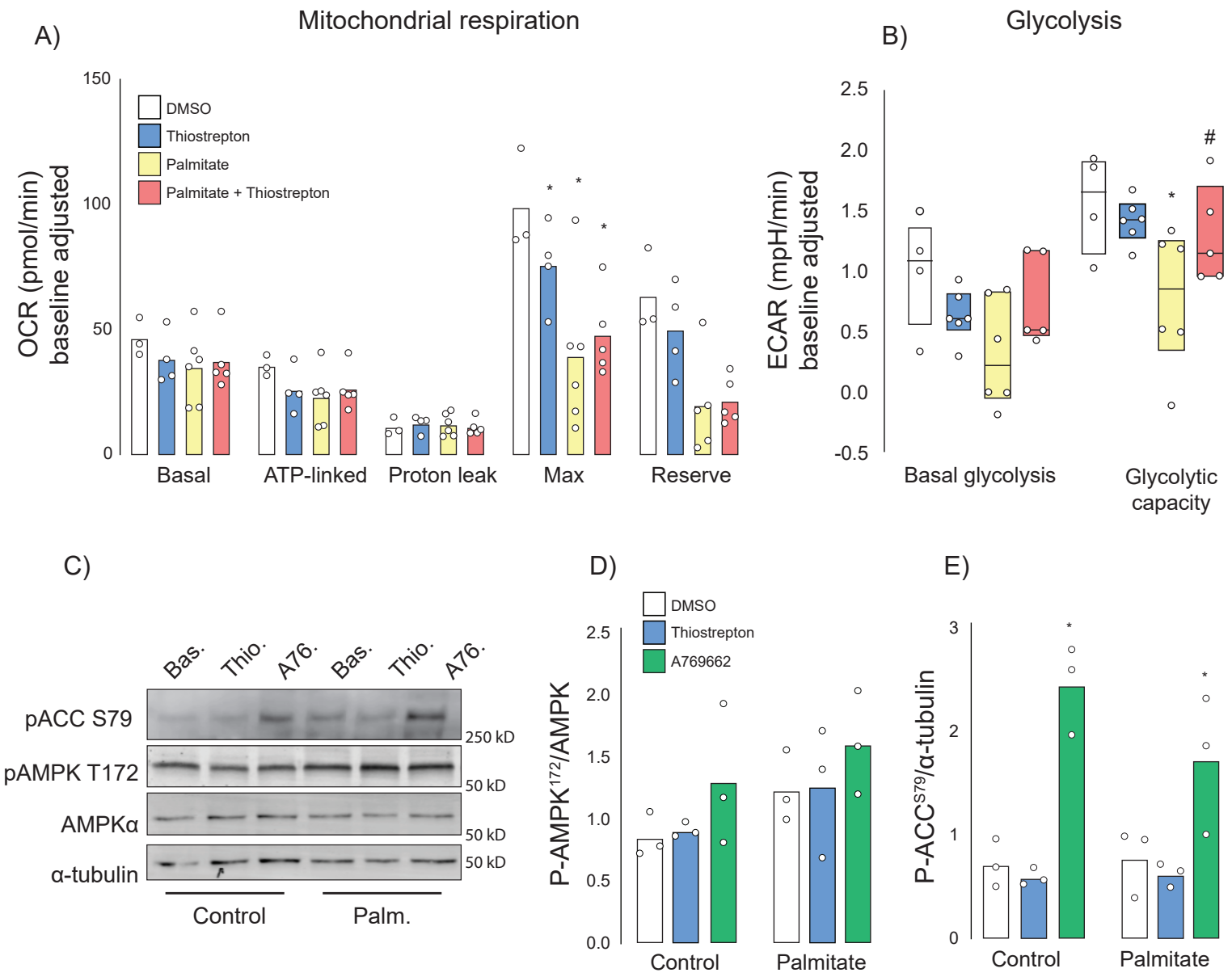
A)
Mitochondrial respiration
OCR (pmol/min) baseline adjusted
150
100
50
0
DMSO
Thiostrepton
Palmitate
Palmitate + Thiostrepton
Basal
ATP-linked
Proton leak
Max
Reserve
B)
Glycolysis
ECAR (mpH/min) baseline adjusted
2.5
2.0
1.5
1.0
0.5
0.0
-0.5
#
Basal glycolysis
Glycolytic capacity
C)
Bas.
Thio.
A76.
Bas.
Thio.
A76.
pACC S79
pAMPK T172
AMPKα
α-tubulin
250 kD
50 kD
50 kD
50 kD
Control
Palm.
D)
DMSO
Thiostrepton
A769662
P-AMPK172/AMPK
2.5
2.0
1.5
1.0
0.5
0.0
Control
Palmitate
E)
P-ACCS79/α-tubulin
3
2
1
0
Control
Palmitate

Supplementary Figure 1: Comparison of linear models

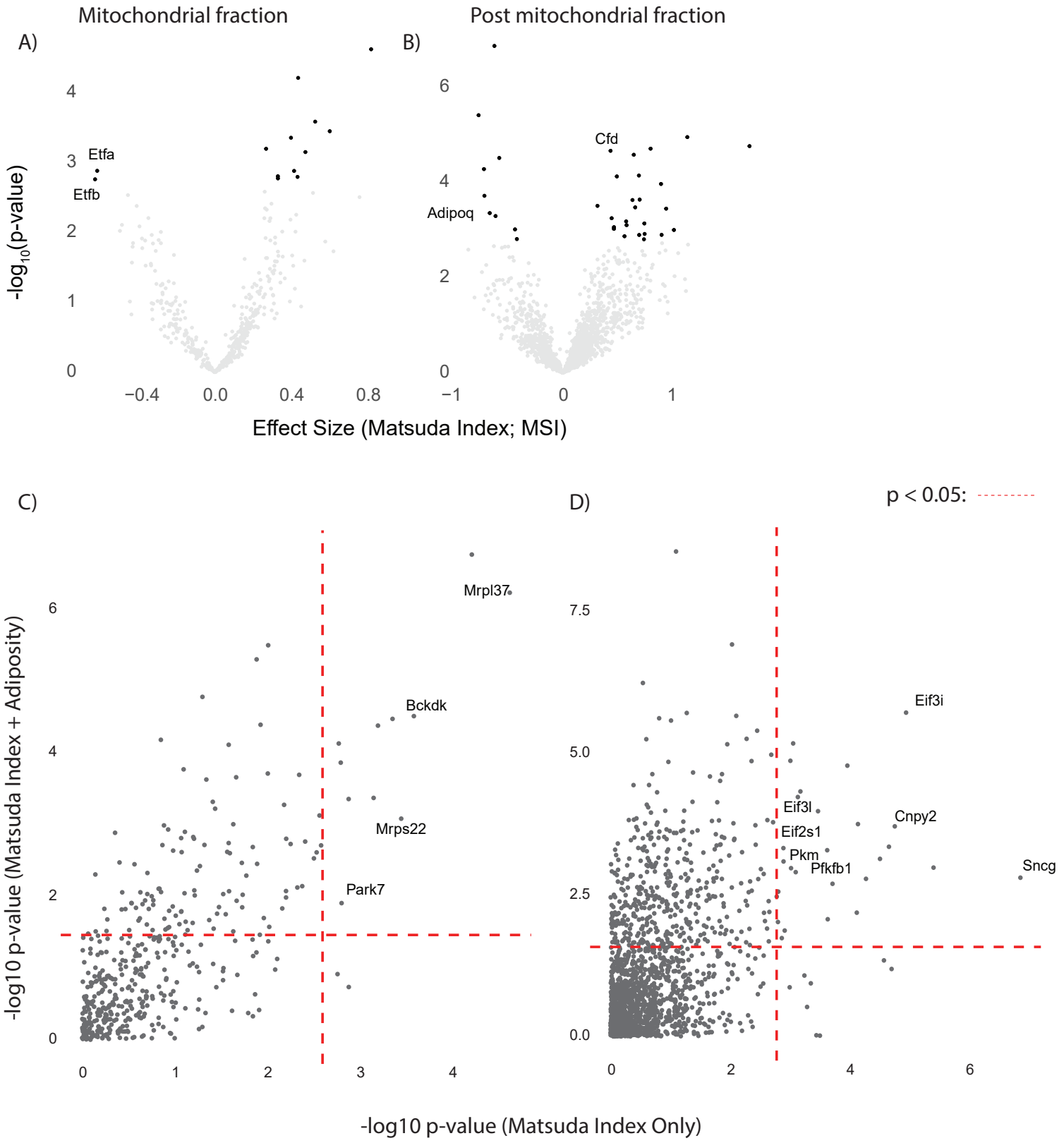

Supplementary Figure 2: Validation of Connectivty Map as a predictor of compound performance

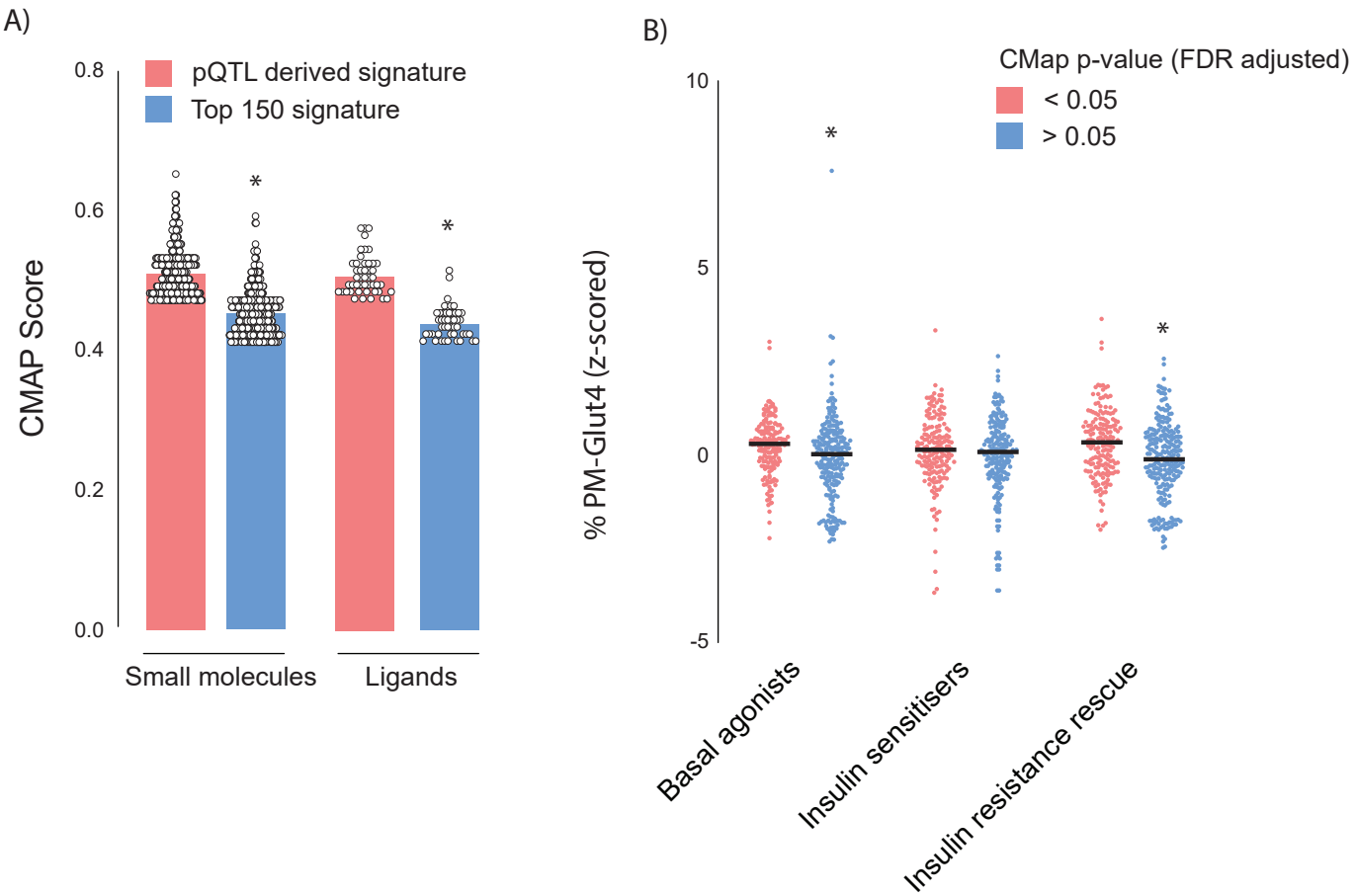

Supplementary Figure 3:

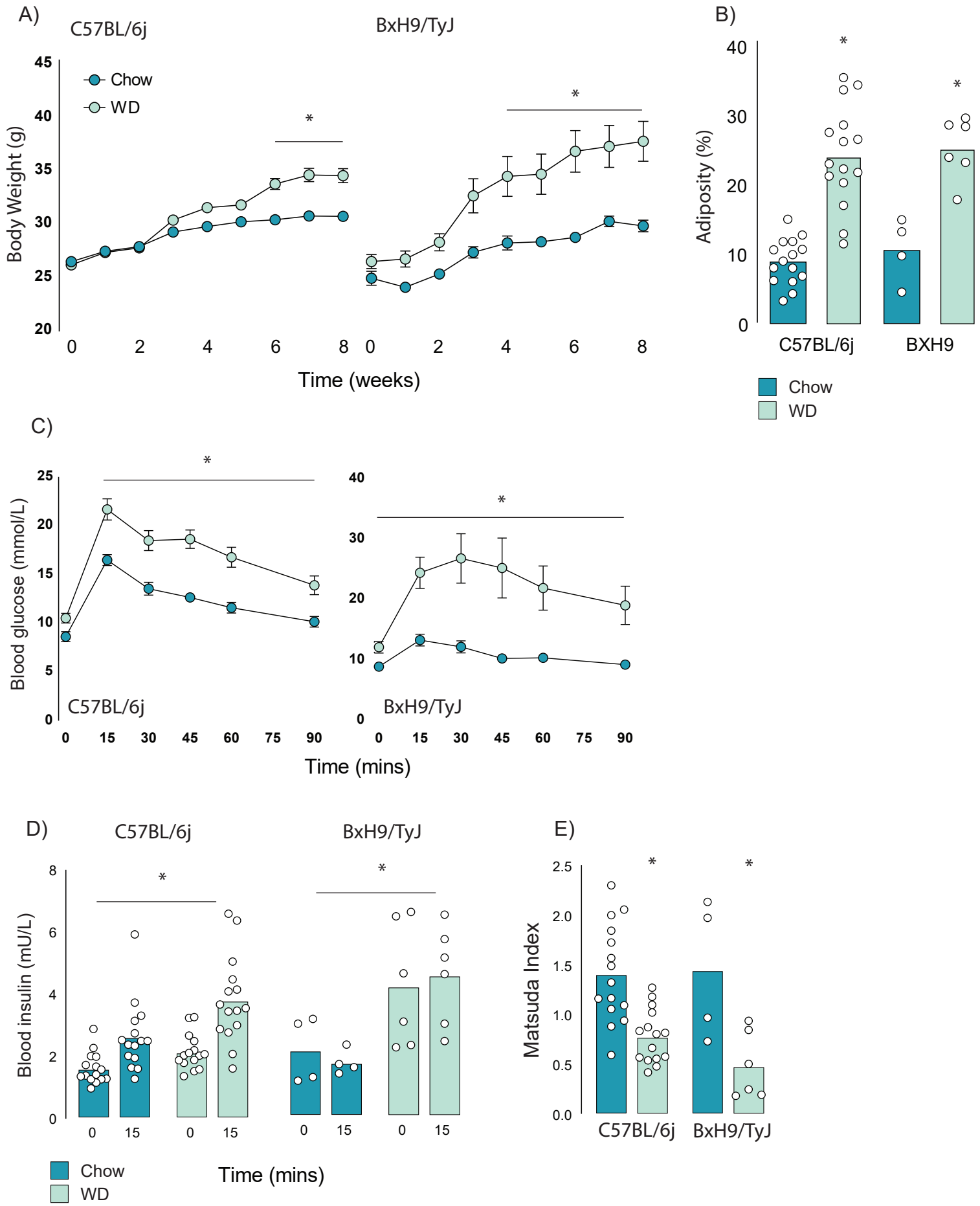

Supplementary Table 1

Symbol	Protein	Effect size
Mtpn	Myotrophin	-1.15
Atox1	Antioxidant 1 copper chaperone	-1.04
Cmpk1	Cytidine monophosphate (UMP-CMP) kinase 1	-1
Tbca	Tubulin cofactor A	-0.92
Pdcd5	Programmed cell death 5	-0.92
Pebp1	Phosphatidylethanolamine binding protein 1	-0.9
Lgals1	Lectin, galactose binding, soluble 1	-0.8
Nagk	N-acetylglucosamine kinase	-0.79
Lzic	Leucine zipper and CTNNBIP1 domain containing	-0.78
Cpne1	Copine I	-0.76
Pgls	6-phosphogluconolactonase	-0.75
S100a6	S100 calcium binding protein A6 (calcyclin)	-0.75
Ndrg2	N-myc downstream regulated gene 2	-0.72
Acyp2	Acylphosphatase 2, muscle type	-0.7
Anxa1	Annexin A1	-0.69
Anxa3	Annexin A3	-0.68
Pdxk	Pyridoxal (pyridoxine, vitamin B6) kinase	-0.68
Dynll2	Dynein light chain LC8-type 2	-0.66
Cltc	Clathrin, heavy polypeptide (Hc)	-0.66
Lta4h	Leukotriene A4 hydrolase	-0.64
Nudcd2	NudC domain containing 2	-0.63
Lamtor5	Late endosomal/lysosomal adaptor, MAPK and MTOR activator 5	-0.63
Fabp5	Fatty acid binding protein 5, epidermal	-0.62
Eps15	Epidermal growth factor receptor pathway substrate 15	-0.61
Gmfb	Glia maturation factor, beta	-0.61
Glrx	Glutaredoxin	-0.58
Tsc22d1	TSC22 domain family, member 1	-0.58
S100a10	S100 calcium binding protein A10 (calpactin)	-0.58
Psma2	Proteasome subunit alpha 2	-0.57
Lgalsl	Galectin like	-0.55
Gnpda1	Glucosamine-6-phosphate deaminase 1	-0.54
Irgq	Immunity-related GTPase family, Q	-0.51
Gamt	Guanidinoacetate methyltransferase	-0.49
Sgcg	Sarcoglycan, gamma (dystrophin-associated glycoprotein)	-0.49
Sod3	Superoxide dismutase 3, extracellular	-0.49
Rap2c	RAP2C, member of RAS oncogene family	-0.49
Letm1	Leucine zipper-EF-hand containing transmembrane protein 1	-0.48
Psmg3	Proteasome (prosome, macropain) assembly chaperone 3	-0.48
Cp	Ceruloplasmin	-0.47
Hpx	Hemopexin	-0.47
Arhgdib	Rho, GDP dissociation inhibitor (GDI) beta	-0.46
Abhd14b	Abhydrolase domain containing 14b	-0.44
Nqo1	NAD(P)H dehydrogenase, quinone 1	-0.44
Phkb	Phosphorylase kinase beta	-0.43
Cstb	Cystatin B	-0.43
Dnajb4	DnaJ heat shock protein family (Hsp40) member B4	-0.41
Hspb2	Heat shock protein 2	-0.41
Adi1	Acireductone dioxygenase 1	-0.4
S100a11	S100 calcium binding protein A11	-0.39
Cpq	Carboxypeptidase Q	-0.39
Hspb3	Heat shock protein 3	-0.38
Anxa4	Annexin A4	-0.38
Nqo2	N-ribosyldihydronicotinamide quinone reductase 2	-0.36
Clta	Clathrin, light polypeptide (Lca)	-0.36
Paics	Bifunctional Phosphoribosylaminoimidazole	-0.35
Wdsub1	WD repeat, SAM and U-box domain containing 1	-0.35
Clpp	Caseinolytic mitochondrial matrix peptidase proteolytic subunit	-0.35
Npl	N-acetylneuraminate pyruvate lyase	-0.34
Snap23	Synaptosomal-associated protein 23	-0.34
Adprhl1	ADP-ribosylhydrolase like 1	-0.34
Apoa4	Apolipoprotein A-IV	-0.32
Gss	Glutathione synthetase	-0.32
Serpina1b	Serine (or cysteine) preptidase inhibitor, clade A, member 1B	-0.32
Itih4	Inter alpha-trypsin inhibitor, heavy chain 4	-0.32
Jpt1	Jupiter microtubule associated homolog 1	-0.31
Gda	Guanine Deaminase	-0.3
Rcn2	Reticulocalbin 2	-0.29
Cox17	Cytochrome c oxidase assembly protein 17, copper chaperone	-0.29
Aspa	Aspartoacylase	-0.29
Hint2	Histidine triad nucleotide binding protein 2	-0.28
Fbn1	Fibrillin 1	-0.28
Serpina1d	Serine (or cysteine) peptidase inhibitor, clade A, member 1D	-0.26
Slc25a19	Solute carrier family 25, member 19	-0.26
Suox	Sulfite oxidase	-0.25
S100a9	S100 calcium binding protein A9 (calgranulin B)	-0.18
Phgdh	3-phosphoglycerate dehydrogenase	-0.06